

Personalized Image Generation via Human-in-the-loop Bayesian Optimization

Rajalaxmi Rajagopalan¹ Debottam Dutta¹ Yu-Lin Wei¹ Romit Roy Choudhury¹

Abstract

Imagine Alice has a specific image x^* in her mind, say, the view of the street in which she grew up during her childhood. To generate that exact image, she guides a generative model with multiple rounds of prompting and arrives at an image x^{p*} . Although x^{p*} is reasonably close to x^* , Alice finds it difficult to close that gap using language prompts. This paper aims to narrow this gap by observing that even after language has reached its limits, humans can still tell when a new image x^+ is closer to x^* than x^{p*} . Leveraging this observation, we develop **MultiBO** (Multi-Choice Preferential Bayesian Optimization) that carefully generates K new images as a function of x^{p*} , gets preferential feedback from the user, uses the feedback to guide the diffusion model, and ultimately generates a new set of K images. We show that within B rounds of user feedback, it is possible to arrive much closer to x^* , even though the generative model has no information about x^* . Qualitative scores from 30 users, combined with quantitative metrics compared across 5 baselines, show promising results, suggesting that multi-choice feedback from humans can be effectively harnessed for personalized image generation.

1. Introduction

Modern diffusion models like FLUX (Labs et al., 2025), StableDiffusion3 (Esser et al., 2024), Lumiere (Bar-Tal et al., 2024) continue to make remarkable advances in image generation. In tandem, users continue to raise the bar, asking for images to not only be of high quality, but to also accurately obey their language prompts; the expectation is that the generated image will match an image x^* that the user has in her mind. Can generative models deliver on this expectation? Perhaps detailed surgery on generative model outputs, using a careful combination of prompting, masking, editing, inpainting, etc. could produce the desired image. However, for most lay users, language based prompting is

the main form of expression and that may be inadequate for hyper-personalization. This is expected because the space of images is much higher dimensional than language, hence a given prompt maps to many possible images. Moreover, humans have limited vocabulary and expressivity in describing an image, so not everyone will be able to perfectly craft the optimal prompt. Finally, in the near term, models that jointly learn language and image representations (e.g., CLIP) are likely to have imperfections, causing further misalignment between language and images. Assuming these are true, it appears that there will be a fundamental gap between the image x^* the user has in mind, and the best image x^{p*} that the user can generate through language prompts p . Can we narrow down this gap for everyday users?

Observe that even after language-based prompting has saturated, if a diffusion model could present some images better than x^{p*} , humans can quite robustly pick the image closest to their target x^* . This preference indication carries valuable information to narrow the gap. We cast this as a human-in-the-loop black box optimization problem with preferential input. The goal is to achieve free-form, training-free and interactive image personalization, specifically when language prompting has neared saturation.

We are not the first to utilize human preference in diffusion models; a rich body of work in the areas of *reward-based alignment*, *preference alignment*, and *reinforcement learning using human feedback (RLHF)* is actively exploring this space of ideas (Xu et al., 2023; Wallace et al., 2024; Yeh et al., 2024; Song et al., 2021). Section 5 discusses them in detail with the closest being DEMON (Yeh et al., 2024), a training-free inference-time approach that optimizes the noise at each t without back propagation, using a stochastic optimization by leveraging Probability Flow ODE (PF-ODE) (Song et al., 2021). Our main departure from past work lies in upgrading user preference to a multi-choice format, allowing the user to select any subset from K image options. This offers much richer information, but absorbing this information into blackbox optimization requires a redesign of the likelihood model and the acquisition function. We conduct this redesign and demonstrate that **MultiBO**'s image generation gets tailored to each individual, is not encumbered by reward-hacking, and does not need offline training using large datasets. Our users have to indeed wait between each round of feedback, but assuming

¹University of Illinois, Urbana-Champaign. Correspondence to: Rajalaxmi Rajagopalan <rr30@illinois.edu>.

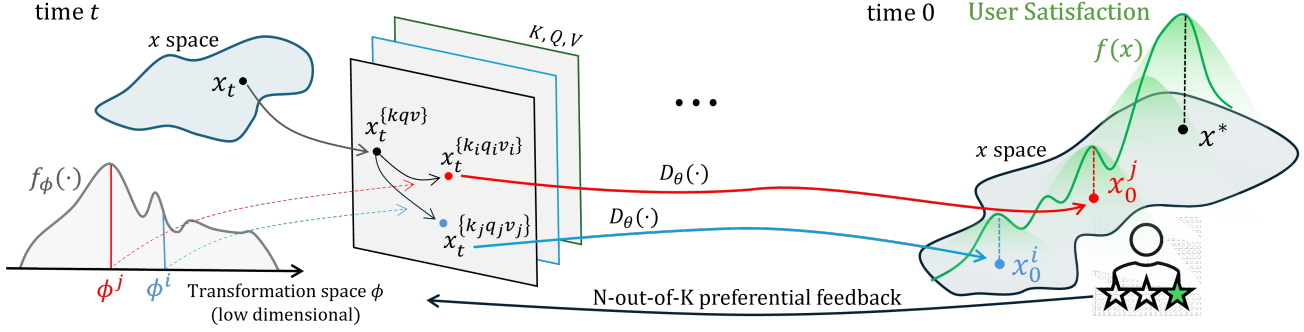


Figure 1. The flow of ideas in **MultiBO**: The BO optimization presents the user with K images and the user chooses N out of K images based on closeness to user’s imagined image x^* . BO accepts the N -out-of- K preferential user feedback and optimizes on the space of transformations applied to the self-attention KQV features, to generate next round of K images, iteratively moving closer to x^* .

that is tolerable, the generated image better approaches the user’s imagined image, x^* . We sketch our core ideas below.

In standard diffusion, $D_\theta(\cdot)$ denoises a noisy image x_t to x_0 . Our goal is to arrive to x^* by performing a human-in-the-loop optimization on x_t as follows:

$$\arg \min_v f(x^*) - f(D_\theta(x_t + v)) \quad (1)$$

Here f is the user’s satisfaction function, maximized at x^* . Unfortunately, $f(\cdot)$ is unknown—a blackbox function—hence there is no gradient to be obtained. However, it is possible to sample $f(\cdot)$, meaning that we can query the user for feedback for any given image $D_\theta(x)$. Using such feedback, we can adopt existing Bayesian optimization (BO) methods using Gaussian Process Regression (GPR), explained in Sec. 2. Briefly, BO will propose judiciously chosen variants of x_t , say x_t^j , and the user will rate how close $D_\theta(x_t^j)$ is to x^* . BO can utilize this feedback to update its predictions, eventually finding \hat{x}_t^* such that $D_\theta(\hat{x}_t^*)$ is arbitrarily close to x^* . Of course, to reduce user burden, the number of user queries needs to be limited to a budget B .

Problems arise in realizing this high level idea. ① Operating BO in the high dimensional pixel space is very difficult. The optimization must be re-cast to a much lower dimensional space, while ensuring that the manifold of correct images, at time t , can be reached from x_t . ② Giving a numerical feedback, $f(D_\theta(x_t^j))$, is known to be difficult for users (Tsukida & Gupta, 2011) because they may not be able to quantify how much worse a given $D_\theta(x_t^j)$ is compared to x^* . However, it is easier to express preferences between pairs or sets of K images. A user-friendly solution must design the BO framework in a suitable low-dimensional space, incorporating the user’s preferential feedback.

Past work have made progress where diffusion models leverage human preference. For example, (Xu et al., 2023; Fan et al., 2023; Wallace et al., 2024) train (global) reward mod-

els, where offline volunteers express preferences between pairs of images; this reward model becomes a proxy for human preference, which ultimately guides the denoising vector. Similar ideas exist in blackbox optimization through preferential likelihood models (Chu & Ghahramani, 2005), where GPR accommodates pairwise preferential feedback from users (more in Sec. 2). However, when the function domain is high dimensional, and when a user’s preference is pairwise, mapping the function reasonably well incurs excessive user feedback. Reducing the user burden calls for richer preferential information, and then integrating them into a lower dimensional space for optimization speed up.

Key Contributions: **MultiBO** contributes by observing that *multi-choice preference queries* bring far richer information to the optimization, and shows that such N -out-of- K feedback can be mathematically accommodated by GPR through an updated likelihood model and acquisition function. Moreover, building on the empirical success of (Nam et al., 2024), **MultiBO** proposes to perform the GPR optimization in a low-dimensional transformation space, where the transformations are applied on $\langle K, Q, V \rangle$ matrices in the attention layer of a diffusion model. The family of transformations are parameterized by ϕ in suitably low dimensions (see Figure. 1), but offer flexibility to explore the image manifold around x_t . In sum, **MultiBO** utilizes multi-choice user feedback to optimize image representations inside the attention layer, empowering users to generate images close to their imagination.

Experiments are designed with a human picking a target image x^* , and a starting image x^{p*} that bears similarity to x^* (i.e., language prompts cannot easily convert x^{p*} to x^*). Five baselines attempt to optimize towards x^* , either with real human feedback, or with their respective (pre-trained) reward models. At the end, each baseline submits their final image \hat{x}^* and 30 external volunteers evaluate the closest match (and other opinion scores). We also use quantitative metrics and a variety of ablations to shed light on the in-

ternal pros and cons of each method, and our own design choices. Results show that **MultiBO** robustly outperforms other methods and there is room for further improvement.

2. Background

■ Bayesian Optimization

Bayesian optimization (BO) (Frazier, 2018; Wang, 2020) is a non-parametric black-box optimization method that consists of two modules:

(1) *Gaussian Process Regression (GPR)*: constructs a probabilistic surrogate of f using the Gaussian likelihood model. The GPR posterior captures our beliefs about the unknown objective function. Given a set of observations $(\mathcal{X}, \mathcal{F})$ and the Gaussian prior kernel, \mathbf{K} , the GPR posterior is defined as,

$$P(\mathcal{F}|\mathcal{X}) \sim \mathcal{N}(\mathcal{F}|\boldsymbol{\mu}, \mathbf{K}) \quad (2)$$

where, $\boldsymbol{\mu} = \{\mu(x_1), \mu(x_2), \dots, \mu(x_K)\}$ is the best model of the function f given the observations $(\mathcal{X}, \mathcal{F})$ and $\mathbf{K}_{ij} = k(x_i, x_j)$, k represents a kernel function, the uncertainty map of f over unsampled regions of the input space.

To make predictions $\hat{\mathcal{F}} = f(\hat{\mathcal{X}})$ at new points $\hat{\mathcal{X}}$, GPR uses the current posterior $P(\mathcal{F}|\mathcal{X})$ to define the joint distribution of \mathcal{F} and $\hat{\mathcal{F}}$, $P(\mathcal{F}, \hat{\mathcal{F}}|\mathcal{X}, \hat{\mathcal{X}})$ as,

$$\begin{bmatrix} \mathcal{F} \\ \hat{\mathcal{F}} \end{bmatrix} \sim \mathcal{N} \left(\begin{bmatrix} \mu(\mathcal{X}) \\ \mu(\hat{\mathcal{X}}) \end{bmatrix}, \begin{bmatrix} \mathbf{K} & \hat{\mathbf{K}} \\ \hat{\mathbf{K}}^T & \hat{\mathbf{K}} \end{bmatrix} \right) \quad (3)$$

where, $\mathbf{K} = k(\mathcal{X}, \mathcal{X})$, $\hat{\mathbf{K}} = k(\mathcal{X}, \hat{\mathcal{X}})$, $\hat{\mathbf{K}} = k(\hat{\mathcal{X}}, \hat{\mathcal{X}})$ and $(\mu(\mathcal{X}), \mu(\hat{\mathcal{X}})) = \mathbf{0}$.

The conditional distribution and hence prediction of $\hat{\mathcal{F}}$ from the joint distribution is,

$$P(\hat{\mathcal{F}}|\mathcal{F}, \mathcal{X}, \hat{\mathcal{X}}) \sim \mathcal{N}(\hat{\mathbf{K}}^T \mathbf{K}^{-1} \mathcal{F}, \hat{\mathbf{K}} - \hat{\mathbf{K}}^T \mathbf{K}^{-1} \hat{\mathbf{K}}) \quad (4)$$

The proof and explanations of all the above are clearly presented in (Wang, 2020)).

(2) *Acquisition function (ACF)*: a sampling strategy that seeks to identify future observations that would improve the likelihood model. The goal, is to use evidence (observations) and prior knowledge (Kernel) to maximize the posterior at each step, so that each new evaluation decreases the distance between the true global maximum and the expected maximum given the GPR model. We use “Expected Improvement” (EI) ACF in this work. Given previous observations $(\mathcal{X}, \mathcal{F})$, let $f^* = \max_{x \in \mathcal{X}} f(x)$ be the current function minimum (i.e., the maximum observed till now). If a new observation $f(x')$ is made at x' , then the new maximum will be either $f(x')$ if $f(x') \geq f^*$ or f^* if $f(x') \leq f^*$.

Hence, the improvement from observing f at x' is

$$[f(x') - f^*]^+.$$

where, $a^+ = \max(a, 0)$.

We want to choose x' that maximizes this improvement. However, $f(x')$ is unknown until the observation is made, so we choose x that maximizes the expectation of this improvement. *Expected Improvement* is thus defined as:

$$\mathbf{EI}(x|\mathcal{X}, \mathcal{F}) = \mathbf{E}[[f(x) - f^*]^+|\mathcal{X}, \mathcal{F}] \quad (5)$$

where, $\mathbf{E}[\cdot|\mathcal{X}, \mathcal{F}]$ is the expectation taken on the GPR posterior distribution (Eqn. 2) given observations $(\mathcal{X}, \mathcal{F})$. Thus, the next sample to make an observation at is:

$$\begin{aligned} x_{\mathbf{EI}} &= \arg \max_{x \in \mathbf{R}^D} \mathbf{EI}(x|\mathcal{X}, \mathcal{F}) \\ &= \arg \max_{x \in \mathbf{R}^D} \mathbf{E}[[f(x) - f^*]^+|\mathcal{X}, \mathcal{F}] \end{aligned} \quad (6)$$

Conventional Bayesian Optimization requires that each function evaluation have a scalar response. However, in applications requiring human judgement, preferences are often more accurate than ratings. The scenario we consider in this work is about presenting two or more samples to a user and requiring only that they indicate preference. This means we cannot query the objective function directly. In this case, f is considered a latent unobservable function, to be inferred from the preferences, which allows for the use of Bayesian optimization approach (Brochu et al., 2010).

■ Preferential Bayesian Optimization

Let us first consider the case of paired preference data i.e., the user is presented two choices to pick one from. A user’s preference information (favoring A over B) can be used to construct a likelihood model. The *probit* likelihood model (Thurstone; Mosteller, 1951) allows us to infer f from the binary preference observations. Assume we have shown the user M pairs of data from a set of N samples $[x_1, \dots, x_N]$. The data set therefore consists of the ranked pairs:

$$\mathcal{X} = \{a_i \succ b_i; i = 1, \dots, M\} \quad a_i, b_i \in \mathcal{Y} \quad (7)$$

Assuming noisy observations, the latent function values are,

$$v(a_i) = f(a_i) + \delta, \quad v(b_i) = f(b_i) + \delta, \quad (8)$$

where, $\delta \sim \mathcal{N}(0, \sigma^2)$ is Gaussian noise. Following the GPR modeling of f (Eqn. 2), The Bradley-Teller-Luce (BTL) (Stein, 1999) model defines the probability that data a is preferred to data b as,

$$\begin{aligned} P(a_i > b_i | f(a_i), f(b_i)) &= \int \int P(a_i > b_i | f(a_i) + \delta_a, f(b_i) + \delta_b) \\ &\quad \cdot \mathcal{N}(\delta_a; 0, \sigma^2) \mathcal{N}(\delta_b; 0, \sigma^2) d\delta_a d\delta_b \\ &= \Phi(z_i) \end{aligned} \quad (9)$$

where $z_i = \frac{f(a_i) - f(b_i)}{\sqrt{2}\sigma}$ and $\Phi(z) = \int_{-\infty}^z \mathcal{N}(\gamma; 0, 1) d\gamma$ is the Gaussian CDF. This preferential likelihood model is called a **Binomial-Probit** regression model. It can be converted to a **Binomial-Logit** model by setting $\varphi(z_i) = \frac{1}{1 + \exp(-z_i)}$.

Given M pairwise observations, The BTL logit likelihood model of observing the preference relations given the latent function values $f(x_i)$ is,

$$P(\mathcal{X}|\mathbf{f}) = \prod_{k=1}^M P(a_i > b_i | f(a_i), f(b_i)) \quad (10)$$

and the GPR posterior is,

$$P(\mathbf{f}|\mathcal{X}) = \frac{P(\mathbf{f})}{P(\mathcal{X})} \prod_{k=1}^M P(a_i > b_i | f(a_i), f(b_i)) \quad (11)$$

where $P(\mathbf{f})$ is the prior, and $P(\mathcal{X}) = \int P(\mathcal{X}|\mathbf{f})P(\mathbf{f})d\mathbf{f}$. The detailed proofs are well established in (Chu & Ghahramani, 2005) and more details are in Appendix A.1.1.

This likelihood serves as the pathway for probabilistic modeling of human preference and its optimization using the Bayesian framework. Thus, BO applied to user preference data is Preferential BO (PBO) (Chu & Ghahramani, 2005).

■ Latent Diffusion Models (LDMs)

Diffusion models generate images via a reverse denoising process. The forward process adds noise to a clean data point x_0 using scales $\bar{\alpha}_t = \prod_i^t \alpha_i$, yielding $x_t = \sqrt{\bar{\alpha}_t} x_0 + (\sqrt{1 - \bar{\alpha}_t}) \epsilon$, where $\epsilon \sim \mathcal{N}(0, I)$ and $x_T \sim \mathcal{N}(0, I)$.

The reverse process recovers the image by modeling $p_\theta(x_{t-1}|x_t)$. This relies on estimating the clean sample \hat{x}_0 using Tweedie's formula and a trained denoiser ϵ_θ :

$$\hat{x}_0 = \frac{x_t - \sqrt{1 - \bar{\alpha}_t} \epsilon_\theta(x_t, t)}{\sqrt{\bar{\alpha}_t}} \quad (12)$$

LDMs improve efficiency by running this process in a VAE-compressed latent space. They enable control (e.g., text-to-image) via conditional denoisers $\epsilon_\theta(x_t, c, t)$, where a domain encoder τ_θ projects prompts c (e.g., CLIP embeddings) for the denoiser.

■ Attention in Diffusion Models

The denoiser network of Diffusion models utilize attention mechanism to prioritize relevant features for consistency and control. Cross-attention aligns visual features with conditioning input c (text), while self-attention models spatial dependencies and global correlations to ensure semantic integrity.

Both mechanisms project image features at time t into query (Q_t), key (K_t), and value (V_t) vectors, yielding the attention map:

$$\text{Attention}(Q_t, K_t, V_t) = \text{Softmax} \left(\frac{Q_t K_t^T}{\sqrt{d}} \right) V_t \quad (13)$$

where $Q_t, K_t, V_t \in \mathbb{R}^{H \times W \times d}$ denote projections across height H , width W , and channels d .

Q and K dictate spatial attributes (Nam et al., 2024). In cross-attention, V connects these to conditioning tokens, whereas in self-attention, V controls non-spatial features (color, texture), enabling fine-grained generation control.

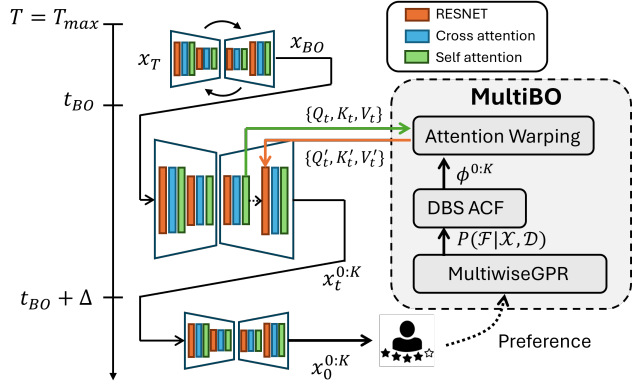


Figure 2. MultiBO Image Personalization Pipeline. **MultiBO** optimizes the self attention Q, K, V features at time interval $[t_{BO}, t_{BO} + \Delta]$ over warping transformation space \mathcal{Y} . At each iteration i , **MultiBO** offers K_i transform parameter choices and the user picks the N “best” option(s) from the corresponding K attention-modified images. The **MultiwiseGPR** likelihood models the unobservable user *satisfaction* function f from the user preferences and the **Dynamic Balanced Subspace** (DBS) acquisition function prescribes the next set of K_{i+1} warp parameters.

3. MultiBO

Briefly, we aim to adjust diffusion generation $x_0 = D_\theta(x_t)$ to closely match a target x^* . We cast this as a human-in-the-loop Black-box optimization (BBO) problem and use Bayesian Optimization (BO) approaches. As discussed in Sec. 2, Preferential Bayesian Optimization (PBO) provides the framework for taking in user feedback in the form of paired preference and modeling unknown *user satisfaction* function f using Pairwise GPR (Eqn. 9). Optimizing the corresponding GPR posterior (Eqn. 11) produces \hat{x}^* .

Two challenges arise in our problem: (1) we can only obtain finite user feedback (typically 50 questions). Therefore, each user preference feedback has to reveal as much information as possible about unknown f . (2) BO has to operate on very high-dimensional RGB Pixel Space to find \hat{x}^* , unsuitable for BBO.

In **MultiBO** we propose two modules: **Multi-choice Preferential Bayesian Optimization** and **Self-Attention Warping** to address these challenges, as illustrated in Figure 2.

Algorithm 1 Personalized Image Generation with **MultiBO**

Input: Prompt P , denoiser ϵ_θ , x_T image sample seed, optimization budget B , Edit time t_{BO} and interval Δ , BO hyperparameters γ , K image choices \mathcal{Z} , User preference $g : x_w > x_{\mathcal{Z}/w}, w \in \{1, \dots, K\}$.

Output: Best image sample \hat{x}^* after B iterations

for $i = 0, \dots, B$ **do**

if $i = 0$ **then**

 Initialize N_0 sets of K random warping parameters
 $\mathcal{X}_0 = (\Theta_1^{(j)}, \Theta_2^{(j)}, \dots, \Theta_K^{(j)}), j = 0, \dots, N_0$

else

$\Theta_{1:K}^{(i)} = \text{DBS}(g, P(\mathbf{f}|\mathcal{X}_i))$; // Next set of choices

$\mathcal{X}_i = [\mathcal{X}_{i-1}, \Theta_{1:K}^{(i)}]$; // Aggregated data

Self Attention Editing:

for $t = t_{BO}, t_{BO} + \Delta$ **do**

$Q_{st}, K_{st}, V_{st} \leftarrow \epsilon_\theta(x_t, t, P)$

$\{Qs'_t, Ks'_t, Vs'_t\}_{1:K} = \text{Warp}(Q_{st}, K_{st}, V_{st}; \Theta_{1:K}^{(i)})$

$\epsilon_{1:K} = \epsilon_\theta(x_t, t, P; \{Qs'_t, Ks'_t, Vs'_t\}_{1:K})$

$\{x_0\}_{1:K} = \text{Sampler}(x_t, t, P, \epsilon_{1:K})$

$g : x_{0,w} > x_{0,\mathcal{Z}/w}$; // Obtain User preference choice

 Fit GPR Posterior $P(\mathbf{f}|\mathcal{X}_i)$ (Eqn. 18)

$Qs_t^*, Ks_t^*, Vs_t^* = \text{Warp}(Q_{st}, K_{st}, V_{st}; \Theta^*)$; // Best params

$\epsilon^* = \epsilon_\theta(x_t, t, P; Qs_t^*, Ks_t^*, Vs_t^*)$,

Best Image: $\hat{x}^* = \text{Sampler}(x_t, t, P, \epsilon^*)$

3.1. Multi-choice Preferential BO (Multi-choicePBO)

In PBO, for the PairwiseGPR model to be a good approximation for f , many observations (preference feedback) are required. An observed pair only provides information about f (resolves uncertainty) for two halves of the input space \mathcal{Y} and more data is needed to sufficiently map the function landscape. This is further exacerbated by increasing dimensionality of the input space. Large number of queries will put considerable burden on the user, diminishing feasibility for human-in-the-loop setting.

To reduce this user burden is to increase the information extracted from each user preference. One way to achieve this is to expand the choice set to K images. This makes intuitive sense, as each observation now resolves f on K partitions of the input space \mathcal{Y} . The user has the flexibility

to choose N -out-of- K best images, $N > 1$ if the user thinks they are equally good or they contain complementary aspects related to the target image. This can significantly bring down the number of user queries at the expense of slight increase in user's cognitive load of selecting N -out-of- K images instead of 1-out-of-2.

To handle this complex preference signal, we design **MultiwiseGPR**, a likelihood model that maps multi-choice preference relations to f and **Dynamic Balanced Subspace (DBS)** acquisition function that supplies the next set of K choices based on the MultiwiseGPR posterior.

■ MultiwiseGPR

We take the discussion on the more general N -out-of- K setting to the Appendix A.1.3. Consider the special case when $N = 1$ i.e., user picks 1 image out of K choices. Consider a set of N distinct samples $x_i \in \mathcal{Y} \subseteq \mathbb{R}^D$; $[x_i : i = 1, \dots, N]$. Let \mathcal{Z} denote the K choices chosen from it for one observation set.

The set of M observed multiwise preference relations on the choice set $\mathcal{Z}_i, i = 1, \dots, M$ is,

$$\mathcal{X}_i = \{a_i^{(w)} \succ \{a_i^{(j)}\}_{j \in \mathcal{Z}_i \setminus w} : i = 1, \dots, M\} \quad (14)$$

where $\{a_i\}_{\mathcal{Z}_i} \in [x_1, \dots, x_N]$ and $a_i^{(w)} \succ \{a_i^{(j)}\}_{j \in \mathcal{Z}_i \setminus w}$ means $a_i^{(w)}$ is the preferred winning sample over $K - 1$ other choices in choice set \mathcal{Z}_i . This preference relationship is modeled by a polycotomous regression model (Held & Holmes, 2006) – multinomial-logit regression model.

Multinomial-Logit Regression: Let us consider the simple case when $M = 1$ observation. There are K samples (images) in the choice set $\{a_1, \dots, a_K\} \in \mathcal{Z}$. We use a Gaussian prior, and the corresponding latent function values are $\mathbf{f} = (f(a_1), \dots, f(a_K))$.

If we assume IID Gaussian noise $\mathcal{N}(0, \sigma)$, then, following Eqn. 8,

$$v_j = f_j + \delta_j, \delta \in \mathcal{N}(0, \sigma)$$

Picking choice $a_i^{(w)}$ out of $\{a_i^{(j)}\}_{j \in \mathcal{Z}_i}, i = 1, \dots, M$ is modeled by a categorical distribution – multinomial-probit (multi-choice version of the binomial in equation 9) as,

$$\begin{aligned} P(Y = w|\mathbf{f}) &= P(v_w = \max_j v_j) \\ &= \int \mathbf{1}\{f_w + \delta_w \geq f_j + \delta_j, \forall j \neq w\} \Phi(\delta) d\delta \end{aligned} \quad (15)$$

where, Y is picking winning index w in K choices \mathcal{Z} . This is a multivariate normal orthant probability (multidimensional CDF). There is no closed-form expression for this multinomial-probit regression model. Following PBO (Chu & Ghahramani, 2005), we replace the probit model for the

logistic model.

Let's update our assumption to IID $\delta \in \text{Gumbel}(0, 1)$ noise in the observation, the multinomial-logit distribution is,

$$P(Y = w|\mathbf{f}) = \frac{\exp(f_w)}{\sum_{j=1}^K \exp(f_j)} \quad (16)$$

The logistic distribution is characterized by the *softmax* function (parallels sigmoidal definition in Eqn. 9). The joint likelihood of observing M multi-choice observations given the latent function values $f(x_i)$ is the product of the likelihood function of each observation in Eqn. 16,

$$P(\mathcal{X}|\mathbf{f}) = \prod_{k=1}^M P(Y = w|\mathbf{f}) \quad (17)$$

and the corresponding Multiwise GPR posterior is,

$$P(\mathbf{f}|\mathcal{X}) = \frac{P(\mathbf{f})}{P(\mathcal{X})} \prod_{k=1}^M P(Y = w|\mathbf{f}) \quad (18)$$

where $P(\mathbf{f})$ is the Gaussian prior, and $P(\mathcal{X}) = \int P(\mathcal{X}|\mathbf{f})P(\mathbf{f})d\mathbf{f}$. The proofs for the likelihood and estimation of the posterior are found in Appendix A.1.2 and (Held & Holmes, 2006).

Thus, we have a probabilistic mapping between multi-choice preference and f that is leveraged by the acquisition function in finding $\hat{x}^* = \arg \max f$.

■ Dynamic Balanced Subspace (DBS):

MultiwiseGPR expects future observations \mathcal{X} that improve the belief of f (Eqn. 18). The naive way is to extend the Expected Improvement (EI) ACF (Eqn. 6) to K -EI i.e., K -jointly maximize the posterior expectation. This joint optimization of an already intractable expectation incurs a tremendous computational load (especially when K is large). In human-in-the-loop settings, we design a light ACF offering K “good” choices that balance observed preferences (*exploitation*) with diverse alternatives (*exploration*).

DBS ACF bypasses the K -EI computational trap by computing only 1 sample, x_{EI} . Armed with x_{EI} and the current best sample \hat{x}^* , DBS ACF constructs a set of K anchor points that act as *bridge vectors* $\mathbf{v}_{\text{bridge}}$ connecting them,

$$\mathbf{v}_{\text{bridge},i} = \hat{x}^* + \gamma_i(x_{\text{EI}} - \hat{x}^*), \gamma_i \in [0, 1] \quad (19)$$

The key intuition is that $\mathbf{v}_{\text{bridge}}$ modulate the explore-exploit trade-off between BO's forward thrust x_{EI} and the belief \hat{x}^* ensuring that the preference set \mathcal{Z} always includes candidates that represent a direct transition from the best known \hat{x}^* to the theoretical optimal global point x_{EI} . The

final K choices (x^+) presented to the user are constructed by random perturbations δ along the $\mathbf{v}_{\text{bridge}}$ directions,

$$x_i^+ = \text{proj}_{\mathcal{Y}}(\mathbf{v}_{\text{bridge},i} + \delta_i), \quad i = 0, \dots, K-1 \quad (20)$$

where $\text{proj}_{\mathcal{Y}}$ is the projection onto the input space $\mathcal{Y} \subseteq \mathbb{R}^D$.

As we are cognizant of the user burden constraints on the optimization especially when the input space $\mathcal{Y} \subseteq \mathbb{R}^D$ is high-dimensional, DBS ACF samples the perturbations $\delta \in \Omega$ from a subspace $\Omega \subseteq \mathcal{Y}$, instead of \mathcal{Y} . Borrowing from the work Bounce (Papenmeier et al., 2023) that performs high-dimensional Bayesian Optimization using embedding spaces of increasing dimensionality, we design our DBS ACF to operate over a subspace constructed dynamically as the optimization proceeds.

Algorithm 2 Dynamic Balanced Subspace (DBS) ACF

Input: BO iteration i ; observed data \mathcal{X}_i ; Current GPR posterior $P(\mathbf{f}|\mathcal{X}_i)$; Current best sample $\hat{\Theta}^*$; Warp parameter space $\mathcal{Y} \subseteq \mathbb{R}^D$
Output: $\Theta_{0:K-1}^+$ - next set of K warping parameter choices
 Expected Improvement sample: $x^+ = \text{EI}(P(\mathbf{f}|\mathcal{X}_i|\mathcal{Y}))$
 Bridge points:
 $\Theta_{\text{bridge},i} = \hat{\Theta}^* + \gamma_i(\Theta^+ - \hat{\Theta}^*), \gamma_i \in [0, 1]$

Dynamic Subspace Selection:

- Compute gradient matrix \mathbb{C} from MultiwiseGP posterior mean $\mu(\mathbf{x})$ near $\hat{\Theta}^*$: $\hat{\Theta} = \hat{\Theta}^* + \eta$

$$\mathbb{C} = \frac{1}{N} \sum_{i=1}^N \nabla \mu(\hat{\Theta}) \nabla \mu(\hat{\Theta})^T$$

Eigen decomposition: $\lambda, \mathbf{u} = \text{EVD}[\mathbb{C}]$

Target dimensions: $d = \arg \max_j \frac{\lambda_j}{\lambda_{j+1}}$ $j \in \{1, 2, \dots, D\}$ (Spectral Gap)

K choices: $\delta_i = \sigma \sum_{j=1}^d \alpha_{i,j} \sqrt{\lambda_j} \mathbf{u}_j$ $\alpha_{i,j} \in [-1, 1]$
 $\Theta_i^+ = \text{proj}_{\mathcal{Y}}(\Theta_{\text{bridge},i} + \delta_i), \quad i = 0, \dots, K-1$

d-dimensional Subspace: We identify the most influential directions in the D -dimensional input space \mathcal{Y} by constructing an uncentered covariance matrix \mathbb{C} of the GPR posterior gradients. Let $\mu(\mathbf{x})$ denote the posterior mean of the Multiwise GPR model. We estimate \mathbb{C} by averaging the outer products of the gradients at H design points sampled in the neighborhood of the current best point \hat{x}^* as,

$$C = \frac{1}{H} \sum_{i=1}^H \nabla \mu(\mathbf{x}_i) \nabla \mu(\mathbf{x}_i)^T, \quad x_i = \hat{x}^* + \eta \quad (21)$$

We determine the subspace dimension d by the **Spectral Gap**, following the eigendecomposition of \mathbb{C} ,

$$d = \arg \max_i \frac{\lambda_i}{\lambda_{i+1}} \quad i \in \{1, 2, \dots, D\} \quad (22)$$

This identifies the threshold d after which additional dimensions contribute significantly less to the visual change of the image, allowing DBS ACF to adaptively *unlock* more dimensions when the function f landscape is complex and *collapse* to a lower-dimensional space when a few dimensions dominate the visual features. Hence, the d -dimensional subspace Ω represents a d -volume in the D -dimensional input space that contains the most visually significant dimensions. The perturbations δ in Eqn. 20 are now samples from the d -Subspace Ω ,

$$\delta_i = \sigma \sum_{j=1}^d \alpha_{i,j} \sqrt{\lambda_j} \mathbf{u}_j \quad (23)$$

where, each coordinate $\alpha_{i,j} \in [-1, 1]$ is *Eigen-Weighted* by scaling with corresponding eigenvalue λ_j . This ensures that perturbations along the most sensitive dimensions are more pronounced than those along dimensions with lower influence.

The eigen weighting and perturbations along the bridge vector ensure that the K choice set of \mathcal{Z} does not collapse into a redundant line between the anchors $\{\hat{x}^*, x_{EI}\}$, i.e., even if x_{EI} and \hat{x}^* are close in the input space, the user is presented with diverse visual variations spanning the most influential latent dimensions of the diffusion model space.

Multi-choice Preferential Optimization provides the framework for translating multi-choice preference data to latent “user satisfaction” function f and optimizing f to ultimately produce $\hat{x}^* = \arg \max f$.

3.2. Self-Attention Warping

Theoretically, Multi-choicePBO would operate on diffusion’s latent space $x_t \in \mathbb{R}^D$. However, this is practically infeasible as the latent space dimensions D are $\approx 16k$. Attention mechanism in diffusion influences both local and global semantic and structural attributes of a generated image. Thus, Multi-choicePBO optimization on the attention features offers the unique opportunity to affect both global and local changes without the dimensionality cost. As the user has already constructed the most expressive prompt, cross-attention features are not relevant to the task at hand. Instead, we optimize on self-attention Q, K, V features that controls spatial features of the image as well as attributes like texture, shape, color, etc.

Keeping the practical constraints of human-in-the-loop optimization in mind, we are interested in further constraining the Multi-choicePBO optimization in Q, K, V space. A reasonable constraint design restricts optimization to valid transformations of the attention space. Since the attention mechanism directly correlates with the pixel-level features of the image, we employ a family of transformations typically applied to images – Warping (Truong et al., 2021).

A **Warping** transform is a functional mapping of each pixel from a reference image to a transformed image. This parallels **MultiBO**’s optimization goal of finding that transformation that maps x_0 to the target x^* .

Affine transformations are linear and provide global alignment; while Thin Plate Spline transforms (TPS) are non-linear deformations that enable local refinement.

Affine: $\mathbf{x}' = A\mathbf{x} + \tau$ where $A \in \mathbb{R}^{2 \times 2}$ and $\tau \in \mathbb{R}^2$.

Thin-Plate Spline (TPS) Transformation: $f(\mathbf{x}) = a_1 + a_x x + a_y y + \sum_{i=1}^N w_i U(\|\mathbf{x} - \mathbf{c}_i\|)$, with $U(r) = r^2 \ln(r^2)$.

MultiBO warps self-attention Q, K, V features using a composed transform of affine and TPS,

$$\text{Affine} + \text{TPS} \quad \text{Composition:} \quad I_q^{\text{warp}1} = \text{Affine}(I_q), \quad I_q^{\text{warp}2} = \text{TPS}(I_q^{\text{warp}1}).$$

Thus, **MultiBO**’s attention optimization problem is,

$$Qs_t^*, Ks_t^*, Vs_t^* = \arg \max_{\Theta \in \mathcal{Y}} \quad \mathbf{W}(Qs_t, Ks_t, Vs_t; \Theta) \\ \text{BO-iters} \leq B \quad (24)$$

where, $\mathbf{W}(\cdot)$ is the warping function, the constrained optimization search space, \mathcal{Y} is the Affine+TPS warping space rather than $\mathbb{R}^{H \times W \times d}$ and t is the diffusion timestep. The optimization framework is Multi-choicePBO. The image personalization pipeline of **MultiBO** is presented in Algorithms 1, and 2.

4. Experiments

■ Datasets:

We curate prompts and corresponding target images x^* from popular prompt datasets in diffusion image editing space like AttendExcite (Chefer et al., 2023), T2ICompBench (Huang et al., 2023b), RareBench (Park et al., 2025) and preference alignment space such as HPSv2 (Wu et al., 2023) benchmark dataset, GenEval (Ghosh et al., 2023), PartiPrompts (Yu et al., 2022), Pick-a-Pic (Kirstain et al., 2023), and Dalle (Zhang et al., 2024a).

■ Baselines:

(1) *Preference Alignment*: We compare with training-based methods: DiffusionDPO (Wallace et al., 2024) and Iter-Comp (Zhang et al., 2024a), training-free methods: DNO (Tang et al., 2024), DAS (Kim et al., 2025), and DEMON (Yeh et al., 2024).

(2) **MultiBO**_{<reward>}: Replace the human scorer with popular reward scores and target-based metrics, CLIP-I2I and LPIPS. This category of baselines is closest to the alignment works except with a different optimization (BO) algorithm.

(3) *L2-guided*: the ideal upper limit, constructed by directly guiding diffusion denoising with classifier guidance in the

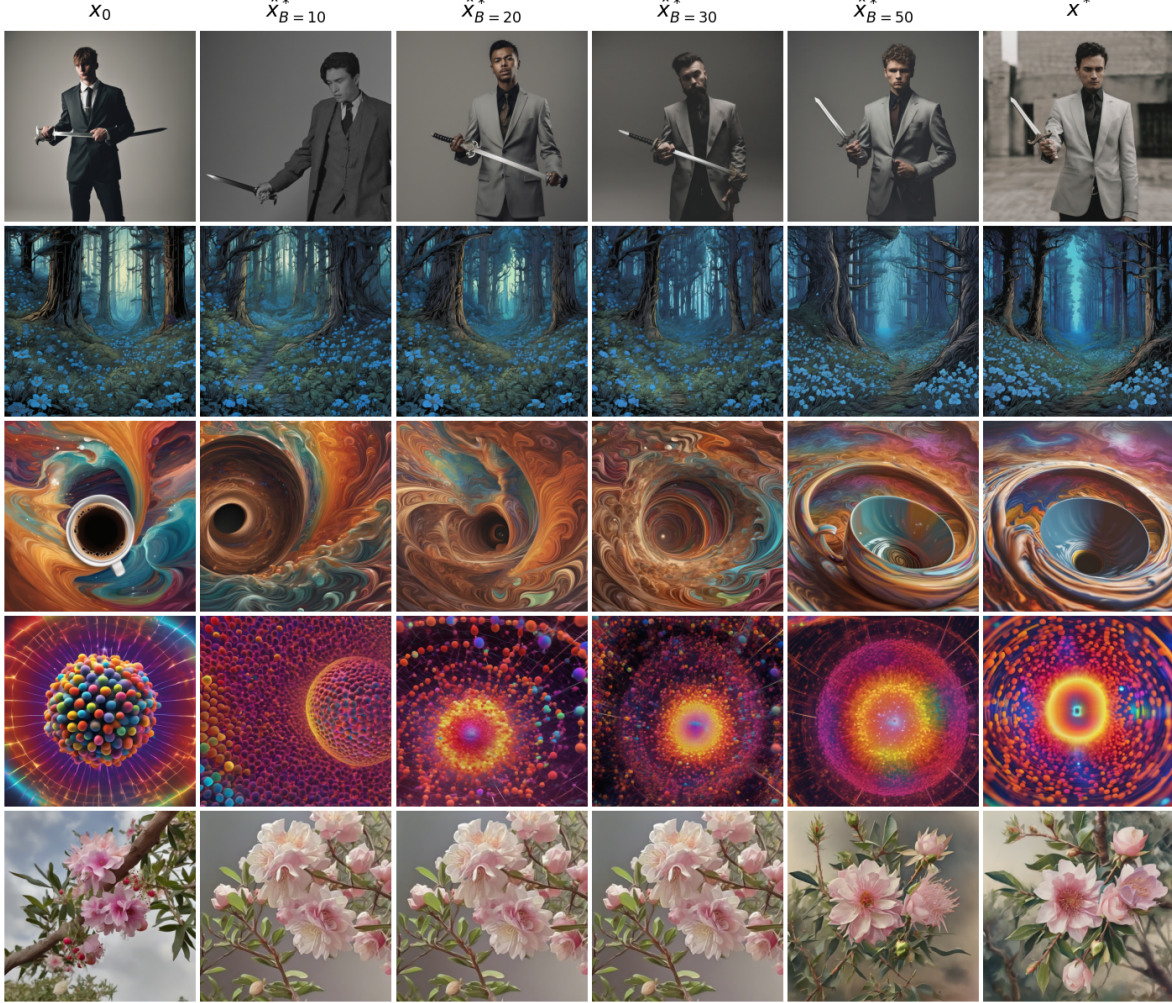


Figure 3. Qualitative Results– **MultiBO** optimization progress: Starting image $x_0 = D_\theta(x_t)$ after prompting, best image \hat{x}^* after $B = 10, 20, 30, 50$ iters, and the true target x^* . For prompts : “A person in a suit holding a sword.”, “A forest with blue flowers illustrated in a digital matte style by Dan Mumford and M.W Kaluta.”, “A swirling, multicolored portal emerges from the depths of an ocean of coffee, with waves of the rich liquid gently rippling outward. The portal engulfs a coffee cup, which serves as a gateway to a fantastical dimension. The surrounding digital art landscape reflects the colors of the portal, creating an alluring scene of endless possibilities.”, “an electron cloud model is displayed in vibrant colors with a light spectrum background, showcasing the probability distribution of electrons around the nucleus. the image resembles digital art with pixelated elements, bringing a modern, educational twist to atomic structure visualization.”, “The fragrant flowers bloomed on the sturdy stem and the thorny bush.”.

form of L2 loss w.r.t target x^* .

(4) **MultiBO_{Subspace}**: We replace attention space optimization with **MultiBO** applied on a $100D$ subspace of x_t (Following (Chen et al., 2024)).

■ Metrics:

We compare **MultiBO** against popular preference alignment reward metrics like PicScore (Kirstain et al., 2023), HPSv2 (Wu et al., 2023), Aesthetic (Schuhmann & Beaumont, 2024), ImageReward (Xu et al., 2023), and VILA (Ke et al., 2023). For target alignment, we use CLIP I2I, and LPIPS w.r.t x^* .

■ Implementation Details:

Diffusion Parameters: We implement **MultiBO** on SDXL (Podell et al., 2023) with DDIM for 50 inference steps and guidance scale = 5.0. **MultiBO** performs attention editing during the first 20% of the denoising steps.

Attention Parameters: We target the middle to later attention layers (the decoder layers in the case of UNets) as they have been shown empirically in (Liu et al., 2024) to produce significant spatial changes without the loss of consistency. Nine grid points define the TPS transformation (Truong et al., 2021). The maximum limits for affine parameters are, translation = 0.75 (75% pixel shift), scaling factor = 4 (scaled up to 4 times or scaled down to 1/4th), and shear and rotation angles are limited to $+/ - \pi/3$.

BO Parameters: **MultiBO**’s optimization is performed for $B = 50$ iterations. $N_0 = 10$ initial Sobol samples to start the optimization. We use Q-NoisyNegativeLogLikelihoodExpectedImprovement (QNoisyNEI), number of restarts = 50, and raw samples = 4096 for finding x_{EI} . In DBS ACF, a spectral gap threshold of $\gamma = 2.0$ is chosen to identify subspace dimension d (Eqn. 22).

We use $K = 4$ preference choice set and ran **MultiBO** for three different seeded trials per prompt/target pair. We ran all experiments on a single NVIDIA A6000 GPU (48GB).

The **MultiBO** image editing pipeline code base and simple inference script is released¹.

4.1. Results

The two key performance goals of **MultiBO**: Alignment with (1) target x^* , (2) general human preference metrics.

1 Alignment with Target x^* :

Figure 3 qualitatively tracks **MultiBO**’s optimization progress. After $B = 50$ iterations, **MultiBO** steers D_θ to produce \hat{x}^* well aligned with x^* . **MultiBO** exhibits superior performance in target-based metrics, CLIP-I2I and LPIPS in Table 1 over all baselines except L2-guided, which is the upper-bound on how close we can get to the target (except DEMON_{LPIPS}). Preference Alignment baselines were not tuned for a particular target so their poor CLIP-I2I and LPIPS performance is expected. However, the more interesting result is that **MultiBO** also beats **MultiBO**_{CLIP-I2I} and **MultiBO**_{LPIPS} (**MultiBO**’s human scorer replaced by the corresponding metric scorer and directly taking target as input). This validates our hypothesis that humans function as sophisticated guidance models, capturing nuances missed by approximate metrics. Notably, users dynamically shift focus between global semantics and precise local spatial control through their preference choices.

Additionally, **MultiBO** significantly outperforms **MultiBO**_{Subspace} on all metrics, implying that constraining the optimization to attention space instead of latent space x_t is prudent to optimize quickly under $B = 50$ queries for human-in-the-loop setting. (Please refer to the Appendix B for qualitative results). Thus, the versatility of human-in-the-loop multi-choice preference coupled with constrained Bayesian Optimization is well suited to address our target alignment task.

2 Alignment with Preference Reward Metrics:

Training-based methods: Table 1 demonstrates **MultiBO**’s comparable performance across most alignment reward met-

rics while substantially outperforming fine-tuned models like DiffusionDPO (Wallace et al., 2024) and IterComp (Zhang et al., 2024a) on ImageReward and Aesthetic metrics, respectively. This is particularly significant considering that DiffusionDPO and IterComp (together with a reward model) are trained on massive datasets of 58,000+ and 55,000+ image pairs—whereas **MultiBO** reaches these results in only $B = 50$ iterations with a single user and no model training. These results confirm that reward models remain mere proxies for human judgment; by involving humans directly, we not only improve derived metrics but also more effectively bridge the gap to true target alignment.

Inference-time methods: Inference-time methods DNO (Tang et al., 2024), DEMON (Yeh et al., 2024), and DAS (Kim et al., 2025) maximize popular reward metrics rather than pursuing target alignment. While DNO and DEMON optimize diffusion noise and DAS employs Sequential Monte Carlo (SMC) to sample aligned distributions, **MultiBO** uses probabilistic optimization. Unlike SMC’s focus on distribution estimation, our BO framework directly identifies the optimum \hat{x}^* , making it uniquely suited for the target alignment task.

For a fair comparison, alongside **MultiBO**, we evaluate {method} \langle reward \rangle pairs against **MultiBO** \langle reward \rangle (where the human is replaced by the corresponding \langle reward \rangle model in the BO loop). The results in Table 1 and Figure 4 reveal three critical insights:

a) Broad Applicability across Rewards: Unsurprisingly, for any given reward, **MultiBO** \langle reward \rangle —along with DNO, DEMON, and DAS operating on that same reward—achieves peak performance for that specific metric (Table 1). **MultiBO** \langle reward \rangle shows consistent cross-reward performance, demonstrating that our optimization framework is broadly applicable and comparable to existing alignment methods in maximizing diverse objectives.

b) Robustness to Reward Hacking: Existing alignment methods are often prone to reward-hacking. As shown in Figure 4, DNO_{Aesthetic} and DAS_{Aesthetic} generate very poor images despite achieving high Aesthetic scores (~ 7.7) in Table 1. In contrast, **MultiBO** avoids this pitfall, maintaining visual integrity where others fail.

c) Efficiency of Human Feedback: The most critical result is that **MultiBO** (with a human scorer), despite not explicitly optimizing for any specific proxy reward, performs comparably to DNO, DAS, and DEMON on their own target metrics. This emphasizes that high-quality user-in-the-loop preference input is superior to proxy metrics. By accounting for user burden as a key design constraint, **MultiBO** successfully extracts this high-value information to achieve robust alignment while remaining practically viable.

For a true analysis of **MultiBO**’s target and reward alignment, we compare against DEMON’s *choose generate*

¹<https://github.com/AnnonAnom125/annonAnomrepo.git>

Table 1. Quantitative comparison of different methods on the personalized image generation task (Top, second best, third best).

	Properties		Target Alignment		Reward Metrics			Image Quality	
	training-free	model-agnostic	CLIP-I (\uparrow)	LPIPS (\downarrow)	AES (\uparrow)	Picscore (\uparrow)	HPSv2 (\uparrow)	ImageReward (\uparrow)	VILA (\uparrow)
L2-guided (Oracle)	✓	✓	0.9811	0.1958	6.2163	0.2201	0.2646	0.5883	0.6158
IterComp	✗	✗	0.8539	0.6988	6.1879	0.2289	0.2712	1.1835	0.6708
DiffusionDPO	✗	✗	0.8365	0.7535	6.2367	0.2245	0.2640	0.6029	0.6560
DEMON _{Aesthetic}	✓	✓	0.8109	0.6785	7.2685	0.2224	0.2644	0.4902	0.6484
DNO _{Aesthetic}	✓	✓	0.6931	0.8487	7.7674	0.1905	0.2517	-0.9815	0.4509
DAS _{Aesthetic}	✓	✓	0.6849	0.8495	7.7032	0.1899	0.2498	-1.2349	0.4514
MultiBO _{Aesthetic}	✓	✓	0.8839	0.6418	7.2313	0.2212	0.2634	0.7299	0.6649
DEMON _{PicScore}	✓	✓	0.8839	0.6742	6.7685	0.2221	0.2637	0.4805	0.6792
DNO _{PicScore}	✓	✓	0.8828	0.6449	6.2013	0.2326	0.2731	0.9812	0.6460
DAS _{PicScore}	✓	✓	0.8758	0.6633	6.2190	0.2321	0.2724	0.9553	0.6425
MultiBO _{PicScore}	✓	✓	0.8877	0.6411	6.2282	0.2286	0.2679	0.8856	0.6752
DEMON _{HPSv2}	✓	✓	0.8472	0.6795	7.2777	0.2218	0.2627	0.4922	0.6721
DAS _{HPSv2}	✓	✓	0.8298	0.7436	5.9925	0.2128	0.2673	0.6852	0.6070
MultiBO _{HPSv2}	✓	✓	0.8818	0.6474	7.1735	0.2230	0.2722	0.8695	0.6806
DEMON _{ImageReward}	✓	✓	0.8520	0.6824	6.7221	0.2232	0.2641	1.1530	0.6642
MultiBO _{ImageReward}	✓	✓	0.8794	0.6468	6.7310	0.2221	0.2664	1.2275	0.6655
DEMON _{LPIPS}	✓	✓	0.9095	0.5907	6.2229	0.2184	0.2623	0.3765	0.6154
MultiBO _{CLIP-12I}	✓	✓	0.9246	0.6479	6.0338	0.2198	0.2639	0.8206	0.6186
MultiBO _{LPIPS}	✓	✓	0.9114	0.5924	6.1711	0.2197	0.2623	0.8414	0.6250
MultiBO _{Subspace}	✓	✓	0.8014	0.6726	6.1818	0.1926	0.2512	0.7863	0.6158
MultiBO (Ours)	✓	✓	0.9364	0.5497	6.6690	0.2266	0.2640	0.8883	0.6723

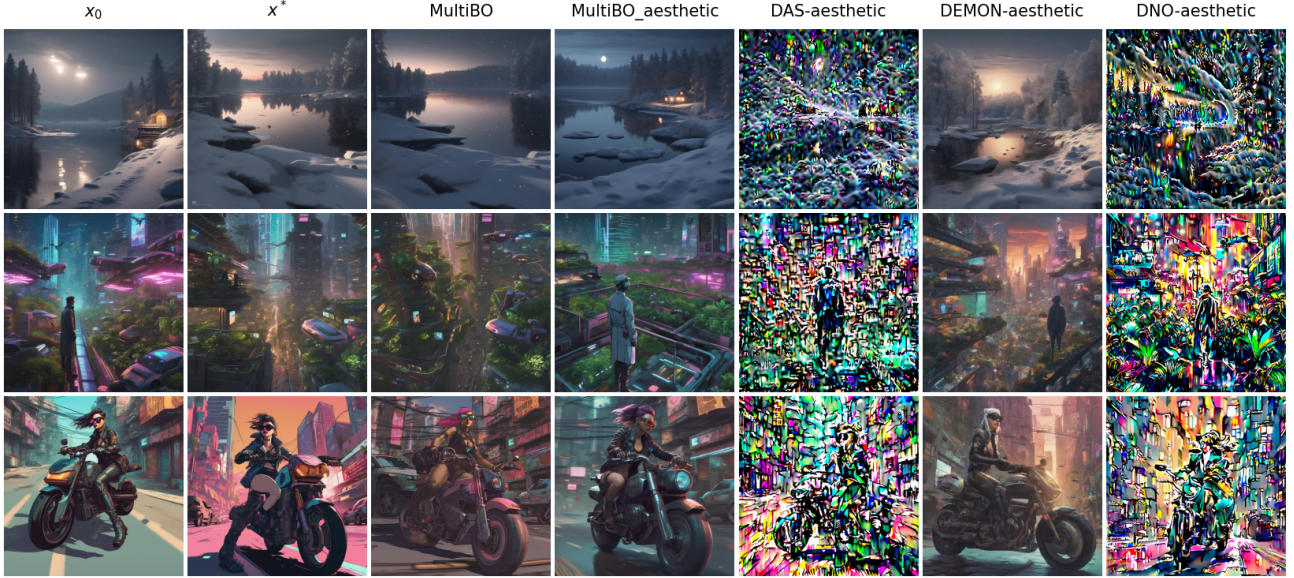


Figure 4. Qualitative comparison of **MultiBO** ($B = 50$), **MultiBO**_{Aesthetic}, **DNO**_{Aesthetic}, **DEMON**_{Aesthetic}, and **DNO**_{Aesthetic}. For prompts: “A vividly realistic depiction of a snowy Swedish lake at night with hyper-detailed, cinematic-level artistry showcased on ArtStation.”, “On the rooftop of a skyscraper in a bustling cyberpunk city, a figure in a trench coat and neon-lit visor stands amidst a garden of bioluminescent plants, overlooking the maze of flying cars and towering holograms. Robotic birds flit among the foliage, digital billboards flash advertisements in the distance.”, “A cyberpunk woman on a motorbike drives away down a street while wearing sunglasses.”

mode, where user selection acts as a non-differentiable reward ($+1/-1$), mirroring our PairwiseGPR formulation (Eqn. 9). Figure 5 shows that **MultiBO** converges closer to x^* within 50 iterations, whereas DEMON stalls around iteration 30. This confirms that naive human-in-the-loop integration is insufficient; effective optimization must balance editing freedom with user burden, which **MultiBO** achieves via MultiwiseGPR and DBS ACF. Furthermore, unlike DEMON’s high-dimensional latent noise (ϵ_t) optimization, **MultiBO** operates in a lower-dimensional attention space, enabling significantly faster alignment.

■ Human Evaluation:

We report human evaluation results from 30 volunteers. Participants were asked to pick the Top-2 methods closest to the target x^* . A method is ranked 1, 2 or 3 (not in top 2). Table 2 demonstrates that **MultiBO** has a high win rate compared to baselines with high user agreement.

Please refer to the Appendix B for additional results including qualitative results on all other reward metrics.

Table 2. Human evaluation results: We report the Win Rate, Mean Rank, and MOS. Kendall’s $W = 0.65$ indicates strong inter-rater agreement.

Method	Win Rate (%) \uparrow	Mean Rank \downarrow	MOS \uparrow
DAS _{PicScore}	0.53	2.98	1.03
DNO _{PicScore}	5.36	2.87	1.25
IterComp	6.49	2.81	1.38
DEMON _{Aesthetic}	9.55	2.79	1.42
MultiBO _{Aesthetic}	11.26	2.73	1.53
DEMON _{choose}	15.60	2.67	1.66
MultiBO _{LPIPS}	31.81	2.36	2.27
MultiBO (Ours)	70.82	1.31	3.58

■ Ablation Studies:

(1) *PairwiseGPR likelihood ($K = 2$) vs MultiwiseGPR ($K > 2$)*: In $B = 50$ steps, Figure 6 and Table 3 illustrate that PairwiseGPR requires far more preference feedback, B to sufficiently span the optimization input space for accurately modeling f and identifying its optimum x^* .

Method	CLIP-I	LPIPS
Pairwise	0.81	0.68
Multiwise	0.94	0.55

Table 3. PairwiseGPR vs MultiwiseGPR performance on target-based metrics

K	LPIPS
4	0.55
6	0.54
10	0.64

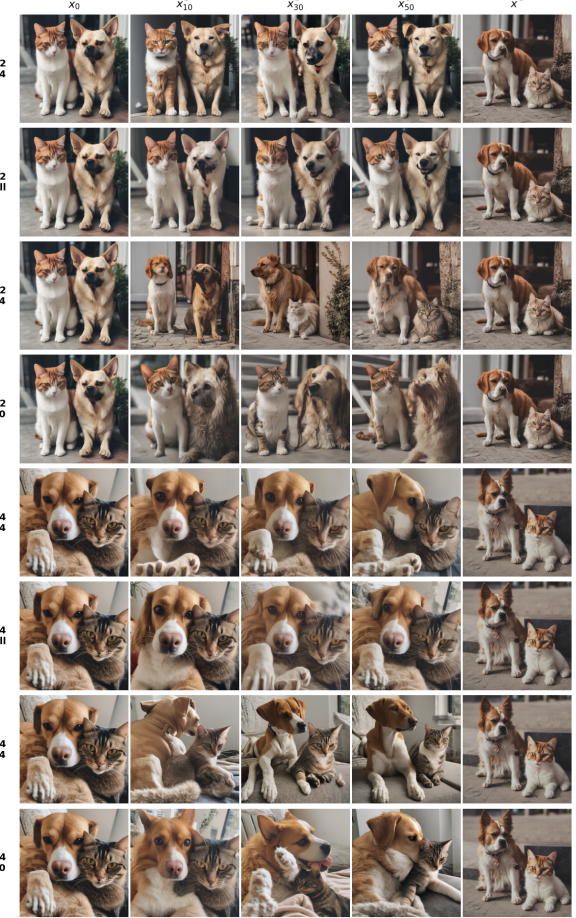
Table 4. **MultiBO** performance for K preference choices

(2) *Number of choices K in choice set \mathcal{Z}* : As number of choices increases, the reliability of user preference drops as they have too much choice, this is reflected in poor metrics reported in Table 4 for $K = 10$. $K = 6$ only fetches marginal gains disproportionate to user burden. $K = 4$

offers good trade-off between informative preference data and minimal user burden.

(3) *Self-Attention Layers to Edit*: Middle to later self-attention layers (decoder layers of UNet) are ideal for spatial and semantic control. The early attention layers do not hold enough semantic structure to cause precise change, often resulting in complete loss of similarity to the source image while the very last layers only result in minute peripheral changes. Figure 7 shows the complete loss of semantic structure when 1 – 24 attention layers of SDXL model are modified and the lack of significant changes when editing layers 64 – 70. Layers 34 – 64 offer the most editing advantage.

Figure 7. Ablation - **MultiBO** applied to different attention layers two different seeds. ($t^+ = 0.0, \Delta = 0.2$, MultiwiseGPR. For prompt: “a cat and a dog”)



(4) *Timesteps to Edit*: Figure 8 identifies that the earlier (T to $0.8T$) we perform edits the more freedom we have in steering the diffusion generation. Editing attention should not be done for prolonged number of timesteps (T to 0) as it steers the diffusion process to low probability points.

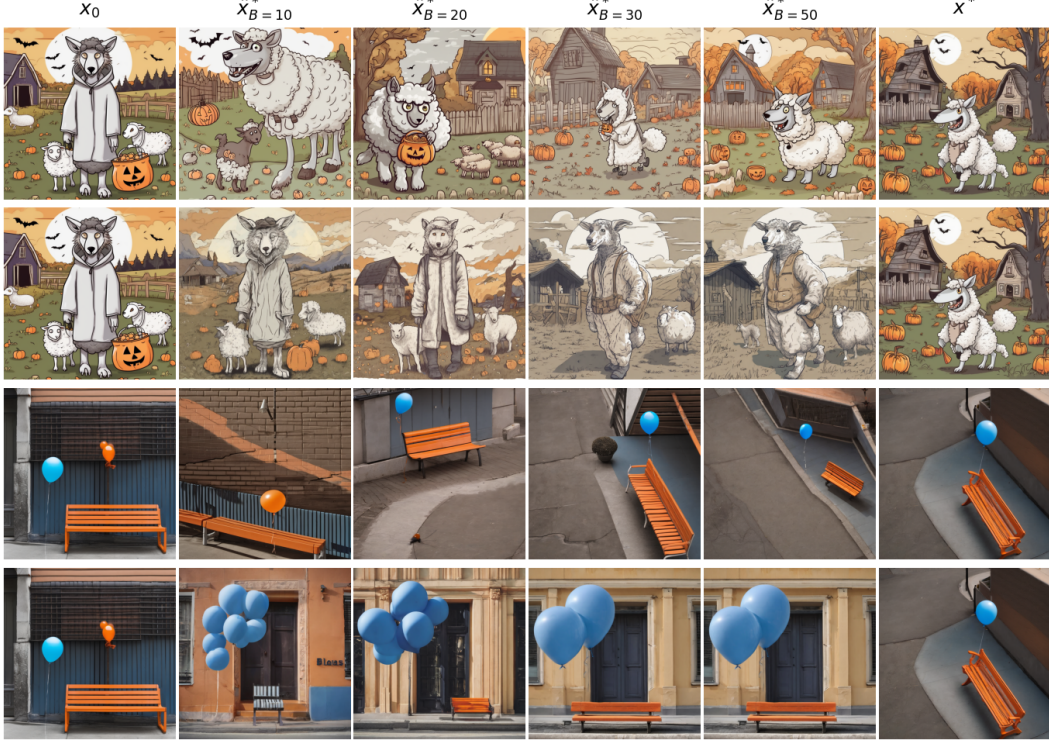


Figure 5. Qualitative results comparing **MultiBO** (1st & 3rd row) and **DEMON choose generate** (2nd & 4th row). For prompts: “A wolf wearing a sheep halloween costume going trick-or-treating at the farm”, “a blue balloon and a orange bench”.

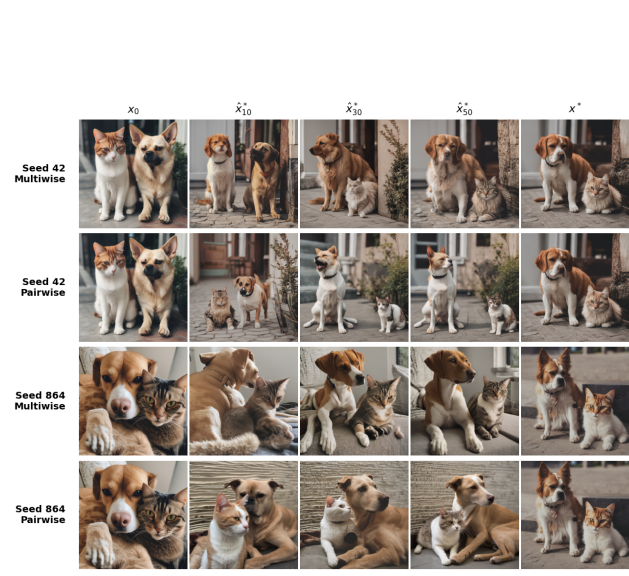


Figure 6. Ablation - Pairwise vs Multiwise Optimization Progress for two different seeds

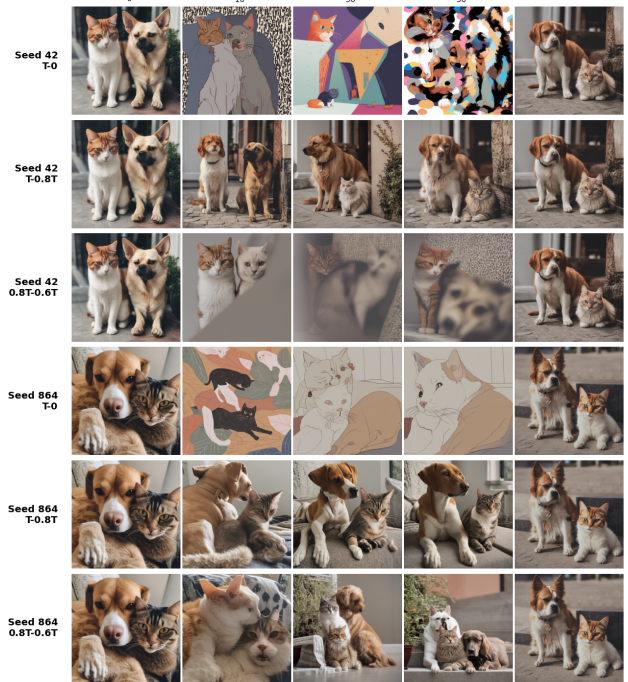


Figure 8. Ablation - **MultiBO** applied at different timesteps t and intervals Δ . (Attn layers 34 – 64, MultiwiseGPR)

5. Related Works

■ **RLHF and Reward Based Methods:** RLHF (Bai et al., 2022; Ouyang et al., 2022) has been extensively adapted for T2I diffusion (Domingo-Enrich et al., 2025; Jiang et al., 2024; Li et al., 2024; Uehara et al., 2024; Zhang et al., 2024b; Lee et al., 2023; Sun et al., 2023). Methods like ImageReward (Xu et al., 2023; Clark et al., 2023; Prabhudesai et al., 2023) use supervised loss with trained reward models. Others like DDPO (Black et al., 2024) and DPOK (Fan et al., 2023; 2024) formulate sampling as a Markov decision process, applying RL to maximize rewards.

■ **Preference Alignment in Diffusion Models:** Aligning diffusion with human preferences is critical for enhancing generation quality and user satisfaction. Direct Preference Optimization (DPO) methods like DiffusionDPO (Wallace et al., 2024) bypass reward model training, directly finetuning on preference data. IterComp (Zhang et al., 2024a) and CaPO (Lee et al., 2025) extend this by iteratively training rewards or calibrating preferences without annotations. To mitigate reward over-optimization, recent works use sample inversion techniques: DDIM-InPO (Lu et al., 2025a), SmPO-Diffusion (Lu et al., 2025b), InversionDPO (Li et al., 2025) reformulate DPO loss using inversion or smoothed distributions. Training-free approaches target inference time. DAS (Kim et al., 2025) uses Sequential Monte Carlo, while DNO (Tang et al., 2024) optimizes noise via reward guidance. DEMON (Yeh et al., 2024) proposes stochastic optimization to guide denoising without backpropagation. However, challenges regarding reward hacking, computational overhead, and personalization persist.

■ **Training-free Attention based Methods:** Attention-based spatial editing employs strategies like feature injection (Zhou et al., 2025; Chen & Huang, 2023; Cao et al., 2023; Huang et al., 2023a; Khandelwal, 2023; Wu et al., 2024; Long et al., 2024; Tumanyan et al., 2023), attention map operations (Wu et al., 2024; Mou et al., 2024), feature concatenation (Balaji et al., 2022; Mou et al., 2023; Deng et al., 2023), cross-modal optimization (Hertz et al., 2022; Esser et al., 2024), and adapter-based re-learning (Ye et al., 2024). Works such as DreamMatcher (Nam et al., 2024) achieves semantic alignment via source Q , K injection and V warping. While effective at reducing inconsistencies, such methods lack free-form editing capabilities, typically relying on source images or custom instructions.

■ **Guidance-based Methods:** Many guidance methods build on the score-based formulation of diffusion models (Song et al., 2021). Classifier Guidance (Dhariwal & Nichol, 2021) requires additional training, works like Universal Guided Diffusion (He et al., 2024; Yoon et al., 2023; Song et al., 2023; Yu et al., 2023; Chung et al., 2023) approximate guidance to use off-the-shelf classifiers or models directly. These methods use Tweedie's formula operate

on the predicted clean sample. However, such methods suffer from poor guidance, and the Tweedie mean prediction quality limits effectiveness in maximizing complex rewards. **Training-free Spatial Editing methods:** InstanceDiffusion (Wang et al., 2024) uses instance-level anchors for specialized object placement and scene construction. Works like (Xie et al., 2023; Phung et al., 2024; Kim et al., 2023; Zhao et al., 2023) use specialized conditioning modalities like bounding boxes, vectors, masks, box-text pairs, custom instructions, etc. to explicitly steer the diffusion generation. These methods place considerable burden on the user to provide these inputs and often perform poorly when a combination of changes are required or when the user is unable to express their requirement. Works like (Yang et al., 2024; Hu et al., 2024) (Yang et al., 2024); (Qu et al., 2023), and (Yu et al., 2025) use Mixture of Experts (MoEs) or LLMs to parse the user requirement into several sub-editing tasks assigned to a specific editing pipeline that excels in that task. Although these methods offer an interactive editing framework they are often limited by the user's capability to express the required changes via syntax like language.

6. Conclusions

We propose **MultiBO**, a training-free, human-in-the-loop image personalization framework built upon Preferential Bayesian Optimization. **MultiBO** addresses the “last-mile” gap between a user’s latent visual intent and the sub-optimal images produced by prompt-based generative models. With only 50 preference queries, the method converges to images that closely align with the user’s ideal target, without requiring any task-specific training data. Query efficiency is further improved by incorporating multi-choice preference feedback and constraining the attention optimization to space of valid warping transformations, substantially reducing the search complexity.

7. Limitations and Future Work

While **MultiBO** achieves good target alignment within a budget B , Figure 17 highlights room for improvement. We diagnose the problem as twofold. First, there are harder scenarios where the generation is reasonably close to the target and the user is forced to choose between equally bad or good choices, i.e., the preference signal weakens, stalling the optimization. Secondly, more iterations $B > 50$ may be needed. This is influenced by the decision to optimize only in the attention domain and restricting to a transformation space, limiting the arsenal of possible changes that can be affected.

For future work, we plan to address these issues by incorporating informed priors into the Gaussian likelihood of BO by leveraging pre-trained reward models. In addition,

we aim to explore customized high-dimensional Bayesian optimization strategies that are better suited to the structure and geometry of latent diffusion representations.

References

Bai, Y., Jones, A., Ndousse, K., Askell, A., Chen, A., Das-Sarma, N., Drain, D., Fort, S., Ganguli, D., Henighan, T., Joseph, N., Kadavath, S., Kernion, J., Conerly, T., El-Showk, S., Elhage, N., Hatfield-Dodds, Z., Hernandez, D., Hume, T., Johnston, S., Kravec, S., Lovitt, L., Nanda, N., Olsson, C., Amodei, D., Brown, T., Clark, J., McCandlish, S., Olah, C., Mann, B., and Kaplan, J. Training a helpful and harmless assistant with reinforcement learning from human feedback, 2022.

Balaji, Y., Nah, S., Huang, X., Vahdat, A., Song, J., Zhang, Q., Kreis, K., Aittala, M., Aila, T., Laine, S., et al. Ediffi: Text-to-image diffusion models with an ensemble of expert denoisers, 2022.

Bar-Tal, O., Chefer, H., Tov, O., Herrmann, C., Paiss, R., Zada, S., Ephrat, A., Hur, J., Liu, G., Raj, A., Li, Y., Rubinstein, M., Michaeli, T., Wang, O., Sun, D., Dekel, T., and Mossner, I. Lumiere: A space-time diffusion model for video generation, 2024. URL <https://arxiv.org/abs/2401.12945>.

Black, K., Janner, M., Du, Y., Kostrikov, I., and Levine, S. Training diffusion models with reinforcement learning, 2024.

Brochu, E., Cora, V. M., and De Freitas, N. A tutorial on bayesian optimization of expensive cost functions, with application to active user modeling and hierarchical reinforcement learning. *arXiv preprint arXiv:1012.2599*, 2010.

Cao, M., Wang, X., Qi, Z., Shan, Y., Qie, X., and Zheng, Y. Masactrl: Tuning-free mutual self-attention control for consistent image synthesis and editing. In *Proceedings of the IEEE/CVF International Conference on Computer Vision*, pp. 22560–22570, 2023.

Chefer, H., Ratzon, O., Paiss, R., and Wolf, L. Attend-and-excite: Attention-based semantic guidance for text-to-image diffusion models. In *ACM SIGGRAPH Conference on Computer Graphics and Interactive Techniques*, 2023.

Chen, S. and Huang, J. Fec: Three finetuning-free methods to enhance consistency for real image editing. In *International Conference on Image Processing, Computer Vision and Machine Learning*, pp. 76–87, 2023.

Chen, S., Zhang, H., Guo, M., Lu, Y., Wang, P., and Qu, Q. Exploring low-dimensional subspaces in diffusion models for controllable image editing, 2024. URL <https://arxiv.org/abs/2409.02374>.

Chu, W. and Ghahramani, Z. Preference learning with gaussian processes. In *Proceedings of the 22nd international conference on Machine learning*, pp. 137–144, 2005.

Chung, H., Kim, J., McCann, M. T., Klasky, M. L., and Ye, J. C. Diffusion posterior sampling for general noisy inverse problems. In *International Conference on Learning Representations*, 2023.

Clark, K., Vicol, P., Swersky, K., and Fleet, D. J. Directly fine-tuning diffusion models on differentiable rewards, 2023.

Deng, Y., He, X., Tang, F., and Dong, W. Z*: Zero-shot style transfer via attention rearrangement, 2023.

Dhariwal, P. and Nichol, A. Diffusion models beat gans on image synthesis. In *Advances in Neural Information Processing Systems*, volume 34, pp. 8780–8794, 2021.

Domingo-Enrich, C., Drozdzal, M., Karrer, B., and Chen, R. T. Q. Adjoint matching: Fine-tuning flow and diffusion generative models with memoryless stochastic optimal control, 2025.

Esser, P., Kulal, S., Blattmann, A., Entezari, R., Muller, J., Saini, H., Levi, Y., Lorenz, D., Sauer, A., Boesel, F., et al. Scaling rectified flow transformers for high-resolution image synthesis. In *Forty-First International Conference on Machine Learning*, 2024.

Fan, Y., Watkins, O., Du, Y., Liu, H., Ryu, M., Boutilier, C., Abbeel, P., Ghavamzadeh, M., Lee, K., and Lee, K. Dpok: Reinforcement learning for fine-tuning text-to-image diffusion models. In *Advances in Neural Information Processing Systems* 36, pp. 79858–79885, 2023.

Fan, Y., Watkins, O., Du, Y., Liu, H., Ryu, M., Boutilier, C., Abbeel, P., Ghavamzadeh, M., Lee, K., and Lee, K. Reinforcement learning for fine-tuning text-to-image diffusion models. In *Advances in Neural Information Processing Systems* 36, 2024.

Frazier, P. I. A tutorial on bayesian optimization. *arXiv preprint arXiv:1807.02811*, 2018.

Ghosh, D., Hajishirzi, H., and Schmidt, L. Geneval: An object-focused framework for evaluating text-to-image alignment. In *Advances in Neural Information Processing Systems (NeurIPS)*, 2023.

He, Y., Murata, N., Lai, C.-H., Takida, Y., Uesaka, T., Kim, D., Liao, W.-H., Mitsufuji, Y., Kolter, J. Z., Salakhutdinov, R., and Ermon, S. Manifold preserving guided diffusion, 2024.

Held, L. and Holmes, C. C. Bayesian auxiliary variable models for binary and multinomial regression. 2006.

Hertz, A., Mokady, R., Tenenbaum, J., Aberman, K., Pritch, Y., and Cohen-Or, D. Prompt-to-prompt image editing with cross attention control, 2022.

Hu, X., Wang, R., Fang, Y., Fu, B., Cheng, P., and Yu, G. Ella: Equip diffusion models with llm for enhanced semantic alignment. *arXiv preprint arXiv:2403.05135*, 2024. URL <https://arxiv.org/abs/2403.05135>.

Huang, J., Liu, Y., Qin, J., and Chen, S. Kv inversion: Kv embeddings learning for text-conditioned real image action editing. In *Chinese Conference on Pattern Recognition and Computer Vision*, pp. 172–184. Springer, 2023a.

Huang, K., Sun, K., Xie, E., Li, Z., and Liu, X. T2i-compbench: A comprehensive benchmark for open-world compositional text-to-image generation. In *Advances in Neural Information Processing Systems (NeurIPS)*, 2023b.

Jiang, Z., Fang, G., Han, J., Lu, G., Xu, H., Liao, S., Chang, X., and Liang, X. Realignndiff: Boosting text-to-image diffusion model with coarse-to-fine semantic re-alignment, 2024.

Ke, J., Ye, K., Yu, J., Wu, Y., Milanfar, P., and Yang, F. Vila: Learning image aesthetics from user comments with vision-language pretraining. In *Proceedings of the IEEE/CVF Conference on Computer Vision and Pattern Recognition (CVPR)*, 2023.

Khandelwal, A. Infusion: Inject and attention fusion for multi-concept zero-shot text-based video editing. In *Proceedings of the IEEE/CVF International Conference on Computer Vision*, pp. 3017–3026, 2023.

Kim, S., Kim, M., and Park, D. Test-time alignment of diffusion models without reward over-optimization. *arXiv preprint arXiv:2501.05803*, 2025.

Kim, Y., Lee, J., Kim, J.-H., Ha, J.-W., and Zhu, J.-Y. Dense text-to-image generation with attention modulation. In *Proceedings of the IEEE/CVF International Conference on Computer Vision (ICCV)*, 2023. URL https://openaccess.thecvf.com/content/ICCV2023/papers/Kim_Dense_Text-to-Image_Generation_with_Attention_Modulation_ICCV_2023_paper.pdf.

Kirstain, Y., Polyak, A., Singer, U., Matiana, S., Penna, J., and Levy, O. Pick-a-pic: An open dataset of user preferences for text-to-image generation. In *Advances in Neural Information Processing Systems (NeurIPS)*, 2023.

Labs, B. F., Batifol, S., Blattmann, A., Boesel, F., Consul, S., Diagne, C., Dockhorn, T., English, J., English, Z., Esser, P., Kulal, S., Lacey, K., Levi, Y., Li, C., Lorenz, D., Müller, J., Podell, D., Rombach, R., Saini, H., Sauer, A., and Smith, L. Flux.1 kontext: Flow matching for in-context image generation and editing in latent space, 2025. URL <https://arxiv.org/abs/2506.15742>.

Lee, K., Liu, H., Ryu, M., Watkins, O., Du, Y., Boutilier, C., Abbeel, P., Ghavamzadeh, M., and Gu, S. S. Aligning text-to-image models using human feedback, 2023.

Lee, K., Li, X., Wang, Q., He, J., Ke, J., Yang, M.-H., Essa, I., Shin, J., Yang, F., and Li, Y. Calibrated multi-preference optimization for aligning diffusion models. In *Proceedings of the Computer Vision and Pattern Recognition Conference*, pp. 18465–18475, 2025.

Li, J., Feng, W., Chen, W., and Wang, W. Y. Reward guided latent consistency distillation. *Transactions on Machine Learning Research*, 2024.

Li, Z., Li, Y., Meng, C., Liu, Z., Yang, L., Zhang, S., Yang, G., Yang, C., Yang, Z., and Sun, L. Inversion-dpo: Precise and efficient post-training for diffusion models. In *Proceedings of the 33rd ACM International Conference on Multimedia*, pp. 9901–9910, 2025.

Liu, B., Wang, C., Cao, T., Jia, K., and Huang, J. Towards understanding cross and self-attention in stable diffusion for text-guided image editing. In *Proceedings of the IEEE/CVF conference on computer vision and pattern recognition*, pp. 7817–7826, 2024.

Long, X., Guo, Y.-C., Lin, C., Liu, Y., Dou, Z., Liu, L., Ma, Y., Zhang, S.-H., Habermann, M., Theobalt, C., and Wang, W. Wonder3d: Single image to 3d using cross-domain diffusion. In *Proceedings of the IEEE/CVF Conference on Computer Vision and Pattern Recognition*, pp. 9970–9980, 2024.

Lu, Y., Wang, Q., Cao, H., Wang, X., Xu, X., and Zhang, M. Inpo: Inversion preference optimization with reparametrized ddim for efficient diffusion model alignment, 2025a.

Lu, Y., Wang, Q., Cao, H., Xu, X., and Zhang, M. Smoothed preference optimization via renoise inversion for aligning diffusion models with varied human preferences, 2025b.

Mosteller, F. Remarks on the method of paired comparisons: I. the least squares solution assuming equal standard deviations and equal correlations. *Psychometrika*, 16(1):3–9, 1951.

Mou, C., Wang, X., Song, J., Shan, Y., and Zhang, J. Dragon-diffusion: Enabling drag-style manipulation on diffusion models, 2023.

Mou, C., Wang, X., Song, J., Shan, Y., and Zhang, J. Diffeditor: Boosting accuracy and flexibility on diffusion-based image editing. In *Proceedings of the IEEE/CVF Conference on Computer Vision and Pattern Recognition*, pp. 8488–8497, 2024.

Nam, J., Kim, H., Lee, D., Jin, S., Kim, S., and Chang, S. Dreammatcher: Appearance matching self-attention for semantically consistent text-to-image personalization. In *Proceedings of the IEEE/CVF Conference on Computer Vision and Pattern Recognition*, pp. 8100–8110, 2024.

Ouyang, L., Wu, J., Jiang, X., Almeida, D., Wainwright, C. L., Mishkin, P., Zhang, C., Agarwal, S., Slama, K., Ray, A., Schulman, J., Hilton, J., Kelton, F., Miller, L., Simens, M., Askell, A., Welinder, P., Christiano, P. F., Leike, J., and Lowe, R. Training language models to follow instructions with human feedback. In *Advances in Neural Information Processing Systems 35*, 2022.

Papenmeier, L., Nardi, L., and Poloczek, M. Bounce: Reliable high-dimensional bayesian optimization for combinatorial and mixed spaces. In *Thirty-seventh Conference on Neural Information Processing Systems*, 2023. URL <https://openreview.net/forum?id=TVD3wNVH9A>.

Park, D., Kim, S., Moon, T., Kim, M., Lee, K., and Cho, J. Rare-to-frequent: Unlocking compositional generation power of diffusion models on rare concepts with LLM guidance. In *The Thirteenth International Conference on Learning Representations*, 2025. URL <https://openreview.net/forum?id=BgxsmVoOX>.

Phung, Q., Ge, S., and Huang, J.-B. Grounded text-to-image synthesis with attention refocusing. In *Proceedings of the IEEE/CVF Conference on Computer Vision and Pattern Recognition (CVPR)*, 2024. URL https://openaccess.thecvf.com/content/CVPR2024/papers/Phung_Grounded_Text-to-Image_Synthesis_with_Attention_Refocusing_CVPR_2024_paper.pdf.

Podell, D., English, Z., Lacey, K., Blattmann, A., Dockhorn, T., Müller, J., Penna, J., and Rombach, R. Sdxl: Improving latent diffusion models for high-resolution image synthesis. *arXiv preprint arXiv:2307.01952*, 2023.

Prabhudesai, M., Goyal, A., Pathak, D., and Fragkiadaki, K. Aligning text-to-image diffusion models with reward backpropagation, 2023.

Qu, L., Wu, S., Fei, H., Nie, L., and Chua, T.-S. Layoutllm-t2i: Eliciting layout guidance from llm for text-to-image generation. *arXiv preprint arXiv:2308.05095*, 2023. URL <https://arxiv.org/abs/2308.05095>.

Schuhmann, C. and Beaumont, R. Laion-aesthetics, 2022, 2024.

Song, J., Zhang, Q., Yin, H., Mardani, M., Liu, M.-Y., Kautz, J., Chen, Y., and Vahdat, A. Loss-guided diffusion models for plug-and-play controllable generation. In *International Conference on Machine Learning*, pp. 32483–32498. PMLR, 2023.

Song, Y., Sohl-Dickstein, J., Kingma, D. P., Kumar, A., Ermon, S., and Poole, B. Score-based generative modeling through stochastic differential equations. In *International Conference on Learning Representations*, 2021.

Stein, M. L. *Interpolation of spatial data: some theory for kriging*. Springer Science & Business Media, 1999.

Sun, J., Fu, D., Hu, Y., Wang, S., Rassin, R., Juan, D.-C., Alon, D., Herrmann, C., van Steenkiste, S., Krishna, R., et al. Dreamsync: Aligning text-to-image generation with image understanding feedback. In *Synthetic Data for Computer Vision Workshop at CVPR 2024*, 2023.

Tang, Z., Peng, J., Tang, J., Hong, M., Wang, F., and Chang, T.-H. Inference-time alignment of diffusion models with direct noise optimization. *arXiv preprint arXiv:2405.18881*, 2024.

Thurstone, L. A law of comparative judgment.

Truong, P., Danelljan, M., Yu, F., and Van Gool, L. Warp consistency for unsupervised learning of dense correspondences. In *Proceedings of the IEEE/CVF international conference on computer vision*, pp. 10346–10356, 2021.

Tsukida, K. and Gupta, M. R. How to analyze paired comparison data. Technical report, 2011.

Tumanyan, N., Geyer, M., Bagon, S., and Dekel, T. Plug-and-play diffusion features for text-driven image-to-image translation. In *Proceedings of the IEEE/CVF Conference on Computer Vision and Pattern Recognition*, pp. 1921–1930, 2023.

Uehara, M., Zhao, Y., Black, K., Hajiramezanali, E., Scalia, G., Diamant, N. L., Tseng, A. M., Levine, S., and Biancalani, T. Feedback efficient online fine-tuning of diffusion models. In *Proceedings of the 41st International Conference on Machine Learning*, volume 235 of *Proceedings of Machine Learning Research*, pp. 48892–48918. PMLR, 2024.

Wallace, B., Dang, M., Rafailov, R., Zhou, L., Lou, A., Purushwalkam, S., Ermon, S., Xiong, C., Joty, S., and Naik, N. Diffusion model alignment using direct preference optimization. In *Advances in Neural Information Processing Systems 37*, pp. 8228–8238, 2024.

Wang, J. An intuitive tutorial to gaussian processes regression. *arXiv preprint arXiv:2009.10862*, 2020.

Wang, X., Rambhatla, S. S., Girdhar, R., Misra, I., and Darrell, T. Instancediffusion: Instance-level control for image generation. In *Proceedings of the IEEE/CVF Conference on Computer Vision and Pattern Recognition (CVPR)*, 2024. URL <https://arxiv.org/abs/2402.03290>.

Wu, J., Bian, J.-W., Li, X., Wang, G., Reid, I., Torr, P., and Prisacariu, V. Gaussctrl: Multi-view consistent text-driven 3d gaussian splatting editing. In *European Conference on Computer Vision*, 2024.

Wu, X., Hao, Y., Sun, K., Chen, Y., Zhu, F., Zhao, R., and Li, H. Human preference score v2: A solid benchmark for evaluating human preferences of text-to-image synthesis, 2023. URL <https://arxiv.org/abs/2306.09341>.

Xie, J., Li, Y., Huang, Y., Liu, H., Zhang, W., Zheng, Y., and Shou, M. Z. Boxdiff: Text-to-image synthesis with training-free box-constrained diffusion. In *Proceedings of the IEEE/CVF International Conference on Computer Vision (ICCV)*, 2023. URL <https://arxiv.org/abs/2307.10816>.

Xu, J., Liu, X., Wu, Y., Tong, Y., Li, Q., Ding, M., Tang, J., and Dong, Y. Imagereward: Learning and evaluating human preferences for text-to-image generation. In *Proceedings of the 37th International Conference on Neural Information Processing Systems*, pp. 15903–15935, 2023.

Yang, L., Yu, Z., Meng, C., Xu, M., Ermon, S., and Cui, B. Mastering text-to-image diffusion: Recaptioning, planning, and generating with multimodal llms. In *Proceedings of the 41st International Conference on Machine Learning (ICML)*, 2024. URL <https://arxiv.org/abs/2401.11708>.

Ye, H., Zhang, J., Liu, S., Han, X., and Yang, W. Ip-adapter: Text compatible image prompt adapter for text-to-image diffusion models, 2024.

Yeh, P.-H., Lee, K.-H., and Chen, J.-C. Training-free diffusion model alignment with sampling demons. *arXiv preprint arXiv:2410.05760*, 2024.

Yoon, T., Myoung, K., Lee, K., Cho, J., No, A., and Ryu, E. K. Censored sampling of diffusion models using 3 minutes of human feedback. In *Advances in Neural Information Processing Systems*, volume 36, 2023.

Yu, J., Xu, Y., Koh, J. Y., Luong, T., Baid, G., Wang, Z., Vasudevan, V., Ku, A., Yang, Y., Ayan, B. K., et al. Scaling autoregressive models for content-rich text-to-image generation. *Transactions on Machine Learning Research*, 2022.

Yu, J., Wang, Y., Zhao, C., Ghanem, B., and Zhang, J. Freedom: Training-free energy-guided conditional diffusion model. In *IEEE/CVF International Conference on Computer Vision*, pp. 23117–23127. IEEE, 2023. doi: 10.1109/ICCV51070.2023.02118.

Yu, Q., Chow, W., Yue, Z., Pan, K., Wu, Y., Wan, X., Li, J., Tang, S., Zhang, H., and Zhuang, Y. Anyedit: Mastering unified high-quality image editing for any idea. In *Proceedings of the Computer Vision and Pattern Recognition Conference*, pp. 26125–26135, 2025.

Zhang, X., Yang, L., Li, G., Cai, Y., Xie, J., Tang, Y., Yang, Y., Wang, M., and Cui, B. Itercomp: Iterative composition-aware feedback learning from model gallery for text-to-image generation, 2024a.

Zhang, Z., Shen, L., Zhang, S., Ye, D., Luo, Y., Shi, M., Du, B., and Tao, D. Aligning few-step diffusion models with dense reward difference learning, 2024b.

Zhao, P., Li, H., Jin, R., and Zhou, S. K. Loco: Locally constrained training-free layout-to-image synthesis. *arXiv preprint arXiv:2311.12342*, 2023. URL <https://arxiv.org/abs/2311.12342>.

Zhou, Y., Gao, X., Chen, Z., and Huang, H. Attention distillation: A unified approach to visual characteristics transfer, 2025.

A. Appendix

A.1. Gaussian Process Likelihoods & Posterior

We derive the GPR likelihood expressions for MultiwiseGPR modeling 1-out-of- K preference choices in A.1.2, and SubsetMultiwiseGPR modeling N -out-of- K preference choices in A.1.3 respectively.

A.1.1. PAIRWISE BINOMIAL LOGIT LIKELIHOOD GPR

The GPR posterior 11 constructed from the binomial likelihood in Eqn 9 has no closed-form expression and although there exist sophisticated variational and Monte Carlo methods, it is typically estimated by Laplace approximation (Brochu et al., 2010). The Laplace approximation follows from Taylor-expansion of the log-posterior of GPR about a set point $\hat{\mathbf{f}} = \mathbf{f}_{\text{MAP}}$, the MAP estimation and is given as,

$$\begin{aligned} \log P(\mathbf{f} | \mathcal{X}) &= \log P(\hat{\mathbf{f}} | \mathcal{X}) + \mathbf{g}^T(\mathbf{f} - \hat{\mathbf{f}}) \\ &\quad - \frac{1}{2}(\mathbf{f} - \hat{\mathbf{f}})^T \mathbf{H}(\mathbf{f} - \hat{\mathbf{f}}) \end{aligned} \quad (25)$$

where, \mathbf{g} , \mathbf{H} are the gradient and Hessian respectively. Their closed form expressions are found in (Chu & Ghahramani, 2005),

A.1.2. MULTIWISE LOGIT LIKELIHOOD GPR

We derive the likelihood expression in Eqn. 16 as follows,

Consider a choice set $\mathcal{Z} = \{1, \dots, K\}$. Each choice $j \in \mathcal{Z}$ is associated with a latent utility

$$v_j = f_j + \delta_j, \quad (26)$$

where $f_j \in \mathbb{R}$ is a true function value and δ_j is random noise. The observed choice is

$$a = \arg \max_{j \in \mathcal{Z}} v_j. \quad (27)$$

The probability that choice i is chosen is

$$\begin{aligned} P(a = i | \mathbf{f}) &= P(v_i \geq v_j \ \forall j \neq i) \\ &= P(f_i + \delta_i \geq f_j + \delta_j \ \forall j \neq i) \\ &= P(\delta_j \leq \delta_i + f_i - f_j \ \forall j \neq i). \end{aligned} \quad (28)$$

$$\begin{aligned} P(a = i | \mathbf{f}) &= \int P(\delta_j \leq \delta_i + f_i - f_j \ \forall j \neq i | \delta_i) p(\delta_i) d\delta_i \\ &= \int \prod_{j \in \mathcal{Z}, j \neq i} F(\delta_i + f_i - f_j) p(\delta_i) d\delta_i, \end{aligned} \quad (29)$$

where $F(\cdot)$ is the CDF of δ_j .

Assume that $\delta_j \sim \text{IID Gumbel}(0, 1)$, with CDF and PDF,

$$F(\delta) = \exp(-e^{-\delta}), \quad p(\delta) = \exp(-(\delta + e^{-\delta})). \quad (30)$$

Substituting them,

$$\begin{aligned} P(a = i | \mathbf{f}) &= \int \prod_{j \in \mathcal{Z}, j \neq i} \exp(-e^{-(\delta_i + f_i - f_j)}) \\ &\quad \exp(-(\delta_i + e^{-\delta_i})) d\delta_i. \end{aligned} \quad (31)$$

Simplifying,

$$\prod_{j \in \mathcal{Z}, j \neq i} \exp(-e^{-(\delta_i + f_i - f_j)}) = \exp\left(-e^{-\delta_i} e^{-f_i} \sum_{j \in \mathcal{Z}, j \neq i} e^{f_j}\right). \quad (32)$$

Thus,

$$P(a = i | \mathbf{f}) = \int \exp\left(-\delta_i - e^{-\delta_i} \left(1 + e^{-f_i} \sum_{j \in \mathcal{Z}, j \neq i} e^{f_j}\right)\right) d\delta_i. \quad (33)$$

Change of variables $t = e^{-\delta_i}$, and $d\delta_i = -dt/t$. The integral becomes,

$$P(a = i | \mathbf{f}) = \int_0^\infty \exp\left(-t \left(1 + e^{-f_i} \sum_{j \in \mathcal{Z}, j \neq i} e^{f_j}\right)\right) dt. \quad (34)$$

which gives,

$$P(a = i | \mathbf{f}) = \frac{1}{1 + e^{-f_i} \sum_{j \in \mathcal{Z}, j \neq i} e^{f_j}} = \frac{e^{f_i}}{\sum_{j \in \mathcal{Z}} e^{f_j}}. \quad (35)$$

Therefore, the multinomial-logit probability is the softmax function (Eqn. 16)

$$P(a = i | \mathbf{f}) = \frac{\exp(f_i)}{\sum_{j \in \mathcal{Z}} \exp(f_j)}. \quad (36)$$

We use Laplace Approximation (Eqn. 25) to estimate the posterior in Eqn. 18. The corresponding gradient and Hessian are,

$$\nabla \log p(\mathbf{f} | \mathcal{X}) = -\mathbf{K}^{-1}\mathbf{f} + \sum_{i=1}^M (\mathbf{e}_{a_i} - \boldsymbol{\pi}_i), \quad (37)$$

$$\nabla^2 \log p(\mathbf{f} | \mathcal{X}) = -\mathbf{K}^{-1} - \sum_{i=1}^M [\text{diag}(\boldsymbol{\pi}_i) - \boldsymbol{\pi}_i \boldsymbol{\pi}_i^\top], \quad (38)$$

where, \mathbf{K} is the GPR prior, \mathbf{e}_{a_i} is the one-hot indicator vector for the observed choice $a_i \in \mathcal{Z}_i$, i.e., the winner

a_i in i th choice set \mathcal{Z}_i is x_j from the set of N samples $[x_1, \dots, x_N]$, $(\mathbf{e}_{a_i})_j = \mathbf{1}[x_j = a_i]$. and,

$$(\pi_i)_j = P(a = x_j | \mathbf{f}) = \frac{\exp(f_j)}{\sum_{k \in \mathcal{Z}_i} \exp(f_k)} \quad (39)$$

is the softmax function.

A.1.3. SUBSET-CHOICE MULTIWISE LOGIT LIKELIHOOD GPR

We consider a more general form of multiwise preference scenario, where instead of selecting one choice, the user selects a *non-empty subset* of the K choices.

Let $\mathcal{Y} = \{x_1, \dots, x_N\}$ be a set of N samples. A single choice set of size K is,

$$\mathcal{Z} = \{a^{(1)}, \dots, a^{(K)}\} \subseteq \mathcal{Y}.$$

The user preference is a non-empty subset

$$A \subseteq \mathcal{Z}, \quad A \neq \emptyset.$$

The observation to the likelihood model is,

$$\mathcal{X} = \{A \succ \emptyset \mid A \subseteq \mathcal{Z}\}.$$

We assume a Gaussian prior over the latent utility function f ,

$$f \sim \mathcal{N}(0, \mathbf{K}),$$

The latent noisy function values are,

$$\mathbf{f} = \{f(x) : x \in \mathcal{Z}\}.$$

$$v(x) = f(x) + \delta,$$

where the noise is IID $\delta \sim \text{Gumbel}(0, 1)$,

Unlike the multinomial-logit model, which assumes a single winning choice, we assume that each element in \mathcal{Z} is independently selected or rejected, and the chosen subset A corresponds to the selected elements.

For a *subset* $A \subseteq \mathcal{Z}$, we define the observed choice as:

$$x_j \in A, \quad v_j \text{ is "chosen".}$$

Assuming IID Gumbel(0, 1) noise, the probability of observing subset A is same as the multinomial-logit derivation in Eqn. 35. The likelihood of a sample x_j to be in the chosen subset $x_j \in A$ is,

$$P(x_j \in A | \mathbf{f}) \propto \exp(f_j),$$

Assuming each sample x_j in choice set \mathcal{Z} is independently selected or not, to be part of subset A , the joint probability of all samples in A is then,

$$\prod_{x_j \in A} \exp(f_j) = \exp\left(\sum_{x_j \in A} f_j\right).$$

The likelihood probability normalization factor (similar to denominator of Eqn. 35) is obtained by summing over all non-empty subsets of \mathcal{Z} as A is one such subset,

$$\sum_{\emptyset \neq C \subseteq \mathcal{Z}} \exp\left(\sum_{x_j \in C} f_j\right).$$

Simplifying,

$$\sum_{C \subseteq \mathcal{Z}} \prod_{x_j \in C} e^{f_j} = \prod_{x_j \in \mathcal{Z}} (1 + e^{f_j}),$$

and removing the empty set case, it becomes,

$$\prod_{x_j \in \mathcal{Z}} (1 + e^{f_j}) - 1.$$

Thus, the likelihood of observing a subset $A \subseteq \mathcal{Z}$ is,

$$P(A | \mathbf{f}) = \frac{\exp\left(\sum_{x_j \in A} f_j\right)}{\prod_{x_j \in \mathcal{Z}} (1 + e^{f_j}) - 1}. \quad (40)$$

This likelihood reduces to the multinomial-logit model (Eqn. 16) when $|A| = 1$.

Given a collection of M observations $\mathcal{X} = \{A_i, \mathcal{Z}_i\}_{i=1}^M$, the posterior distribution is

$$P(\mathbf{f} | \mathcal{X}) = \frac{P(\mathbf{f})}{P(\mathcal{X})} \prod_{i=1}^M P(A_i | \mathbf{f}_{\mathcal{Z}_i}), \quad (41)$$

where $P(\mathbf{f})$ is the GP prior and $P(\mathcal{X}) = \int P(\mathcal{X} | \mathbf{f}) P(\mathbf{f}) d\mathbf{f}$.

Same as MultiwiseGPR with one choice, we use Laplace Approximation (Eqn. 25) to estimate the posterior in Eqn. 41.

We now compute the Gradient and Hessian of the posterior. For a single observation (A, \mathcal{Z}) , we define the indicator vector $\mathbf{Y} \in \{0, 1\}^{|\mathcal{Z}|}$ as,

$$Y_j = \begin{cases} 1, & x_j \in A, \\ 0, & \text{otherwise.} \end{cases}$$

The gradient and Hessian are,

$$\nabla \log p(\mathbf{f} | \mathcal{X}) = -\mathbf{K}^{-1}\mathbf{f} + \sum_{i=1}^M (\mathbf{Y}_i - \boldsymbol{\pi}_i). \quad (42)$$

$$\nabla^2 \log p(\mathbf{f} | \mathcal{X}) = -\mathbf{K}^{-1} - \sum_{i=1}^M \boldsymbol{\Gamma}_i. \quad (43)$$

where, π_j are defined as,

$$\begin{aligned}\pi_j &= P(x_j \in A \mid \mathbf{f}) \\ &= \frac{\sum_{\emptyset \neq C \subseteq \mathcal{Z}, C \ni x_j} \exp(\sum_{x \in C} f(x))}{\sum_{\emptyset \neq C \subseteq \mathcal{Z}} \exp(\sum_{x \in C} f(x))}.\end{aligned}\quad (44)$$

where, $\emptyset \neq C_i \subseteq \mathcal{Z}_i, C_i \ni x_j$ means valid non-empty subsets of \mathcal{Z}_i that contain x_j in them (For M observations, we have $(\pi_i)_j$).

The Hessian diagonal and off-diagonal entries are,

$$\begin{aligned}\Gamma_{jj} &= \pi_j(1 - \pi_j), \\ \Gamma_{jk} &= \pi_{jk} - \pi_j \pi_k, \quad j \neq k,\end{aligned}\quad (45)$$

where,

$$\pi_{jk} = P(x_j, x_k \in A \mid \mathbf{f})$$

B. More Qualitative Results

We show qualitative results for **MultiBO**, **MultiBO**_{<reward>}, training methods like DiffusionDPO (Wallace et al., 2024) and IterComp (Zhang et al., 2024a) and inference time methods, DNO (Tang et al., 2024), DAS (Kim et al., 2025), DEMON (Yeh et al., 2024) operating on different < reward > metrics. These results complement the quantitative counterparts reported in Table 1 in the main paper.

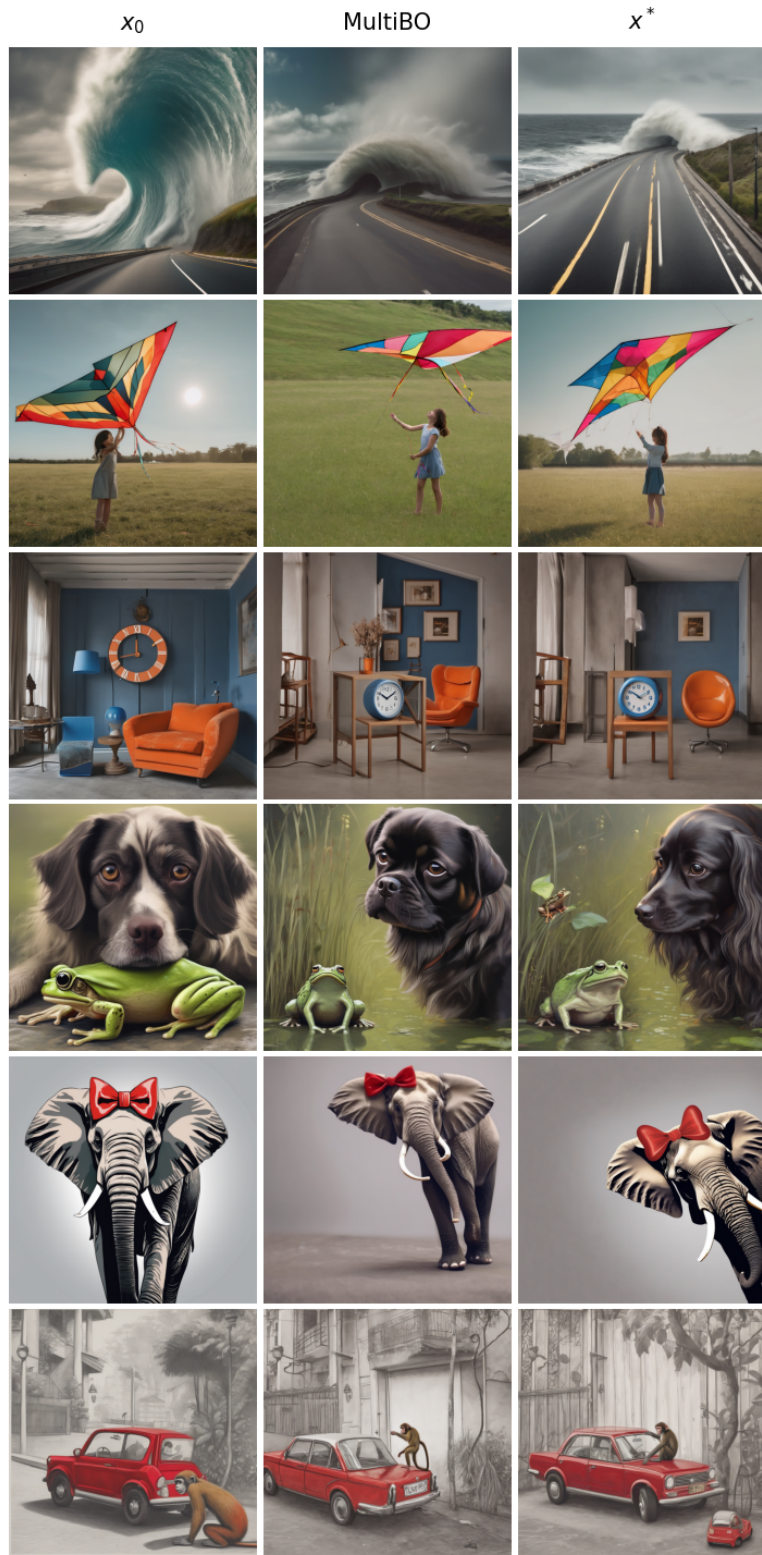


Figure 9. Qualitative results of **MultiBO** ($B = 50$). For prompts: "a tidal wave approaching a coastal road", "A girl is holding a large kite on a grassy field.", "a orange chair and a blue clock", "a dog and a frog", "a elephant and a bow", "a monkey and a red car".

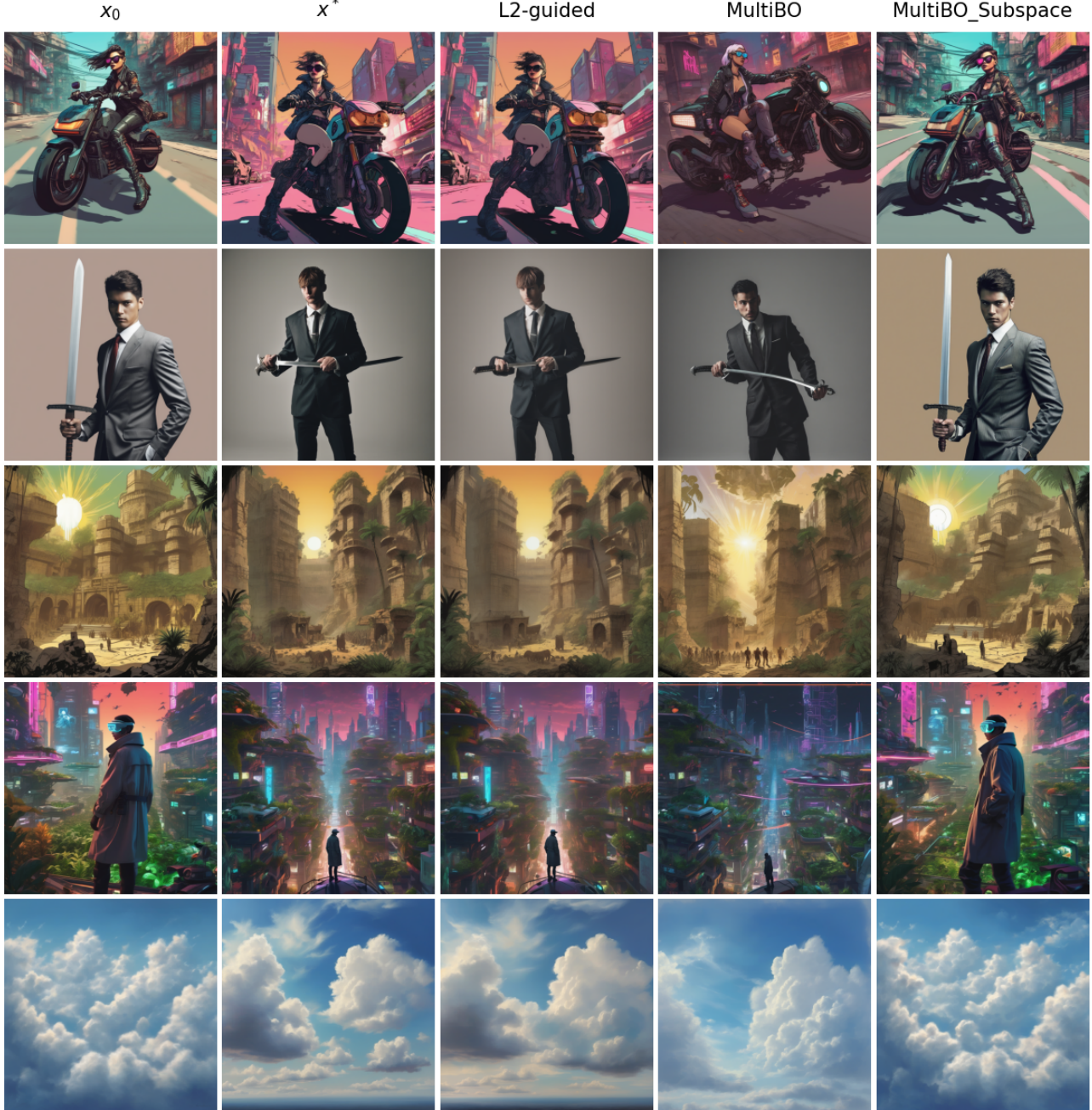


Figure 10. Qualitative results comparing **MultiBO** ($B = 50$), L2-guided, and **MultiBO**_{Subspace}. For prompts: “A cyberpunk woman on a motorbike drives away down a street while wearing sunglasses.”, “A person in a suit holding a sword.”, “A comic book illustration by John Kirby depicting a jungle fortress surrounded by dirt walls in a marketplace setting with cinematic rays of sunlight.”, “On the rooftop of a skyscraper in a bustling cyberpunk city, a figure in a trench coat and neon-lit visor stands amidst a garden of bio-luminescent plants, overlooking the maze of flying cars and towering holograms. Robotic birds flit among the foliage, digital billboards flash advertisements in the distance.”, “The soft, fluffy clouds drifted lazily across the blue sky, a canvas of endless possibilities and imagination.”

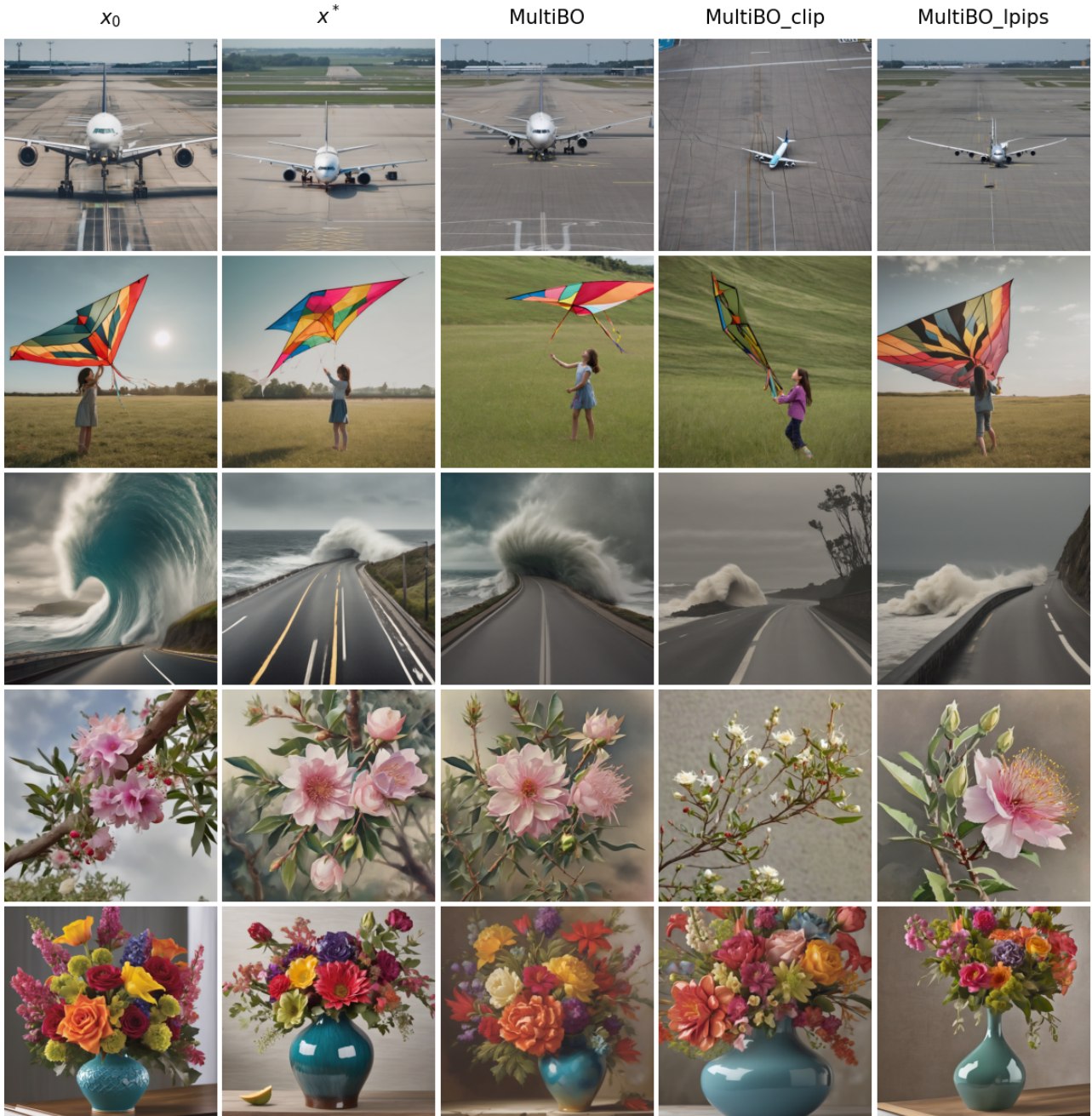


Figure 11. Qualitative results comparing **MultiBO** ($B = 50$), **MultiBO_{CLIP-I}**, and **MultiBO_{LPIPS}**. For prompts: “An airplane on the runway of an airport.”, “A girl is holding a large kite on a grassy field.”, “a tidal wave approaching a coastal road”, “The fragrant flowers bloomed on the sturdy stem and the thorny bush.”, “The smooth, glossy finish of the ceramic vase accentuated the vibrant colors of the flowers, a stunning centerpiece of beauty.”

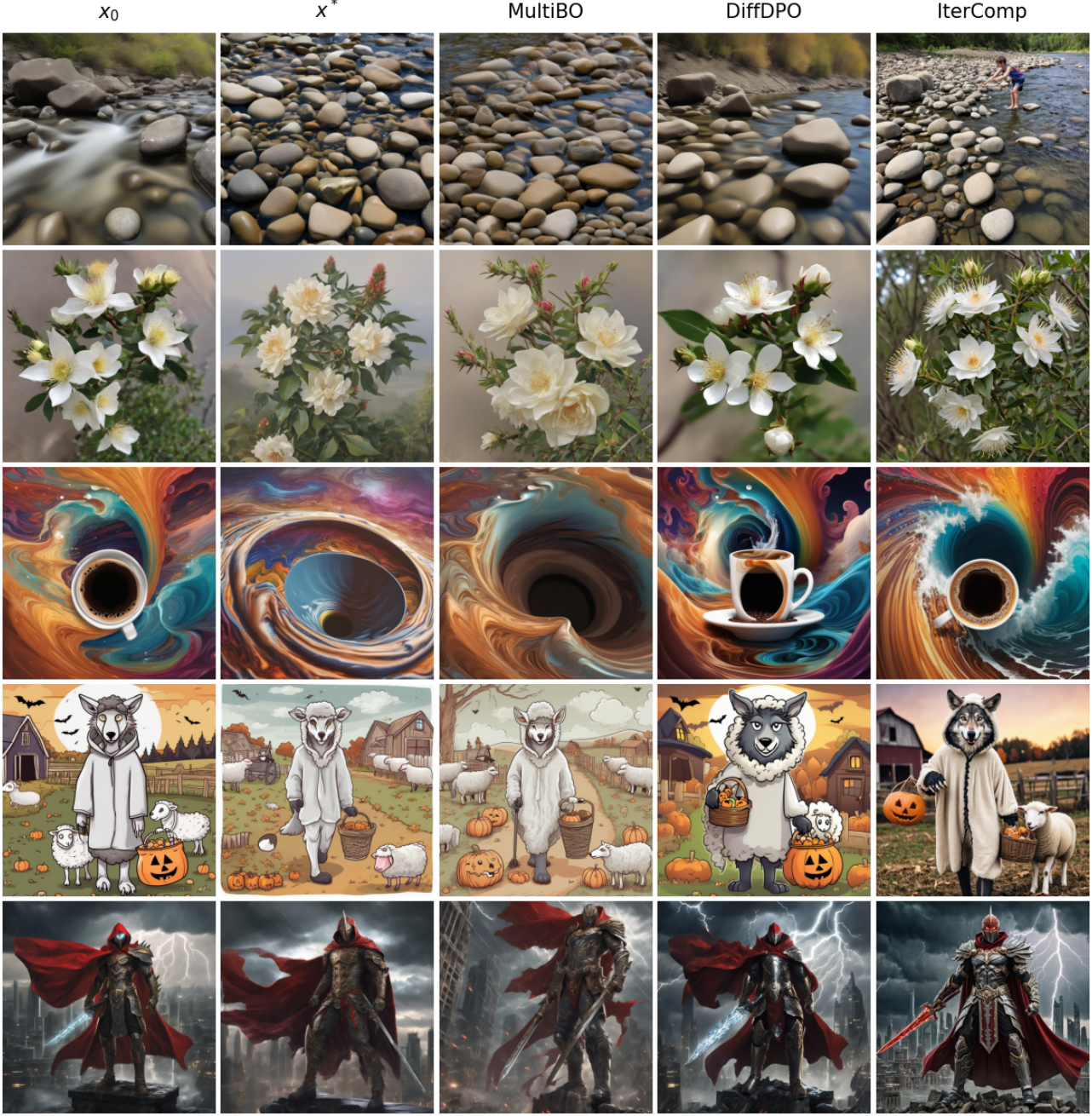


Figure 12. Qualitative results comparing **MultiBO** ($B = 50$), DiffusionDPO, and IterComp. For prompts: “*The smooth, cool surface of the river rocks were perfect for skipping across the water's surface.*”, “*The fragrant flowers bloomed on the sturdy stem and the thorny bush.*”, “*A swirling, multicolored portal emerges from the depths of an ocean of coffee, with waves of the rich liquid gently rippling outward. The portal engulfs a coffee cup, which serves as a gateway to a fantastical dimension. The surrounding digital art landscape reflects the colors of the portal, creating an alluring scene of endless possibilities.*”, “*A wolf wearing a sheep halloween costume going trick-or-treating at the farm*”, “*Amidst a stormy, apocalyptic skyline, a masked warrior stands resolute, adorned in intricate armor and a flowing cape. Lightning illuminates the dark clouds behind him, highlighting his steely determination. With a futuristic city in ruins at his back and a red sword in hand, he embodies the fusion of ancient valor and advanced technology, ready to face the chaos ahead.*”

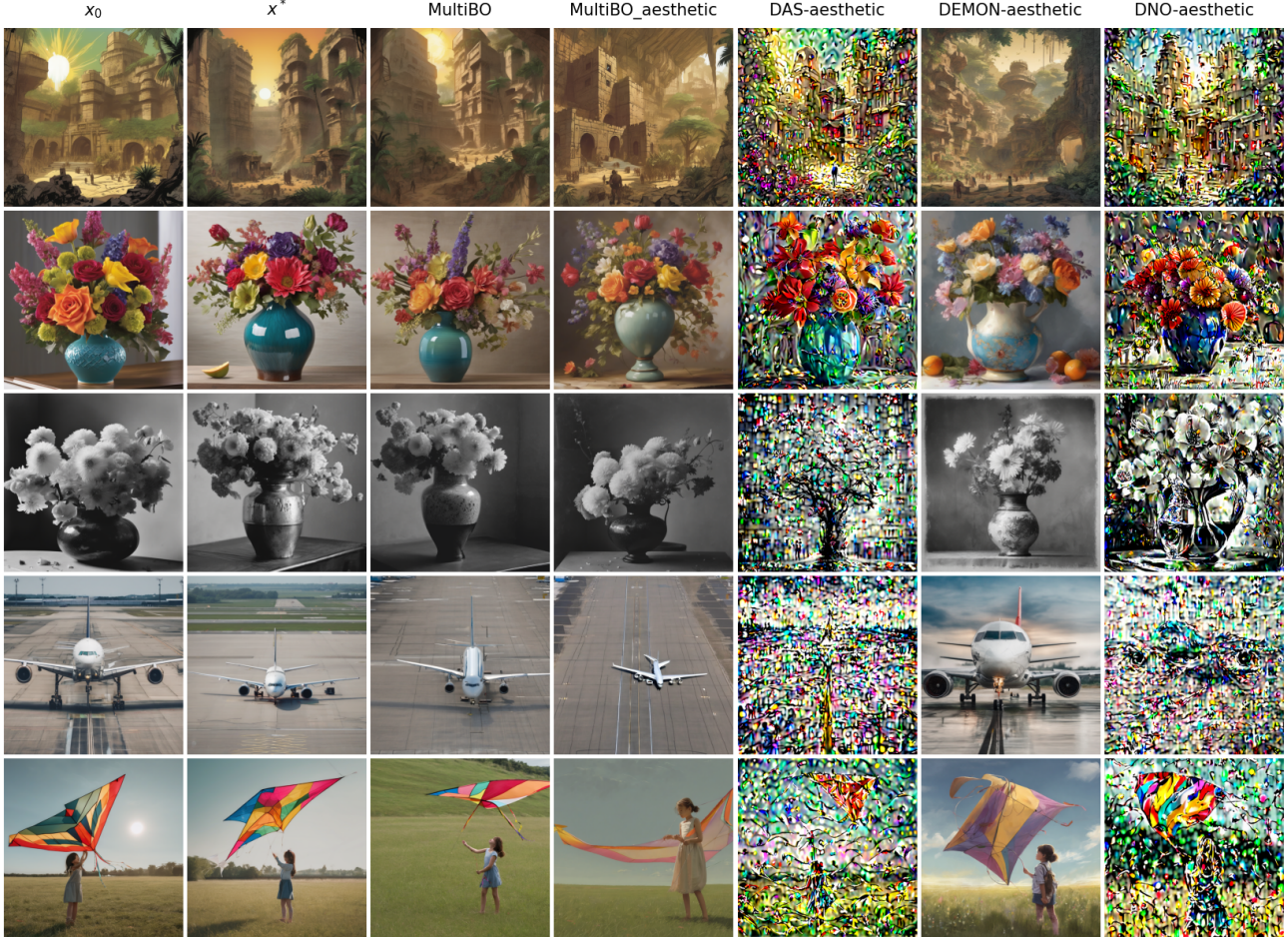


Figure 13. Qualitative results comparing **MultiBO** ($B = 50$), **MultiBO_{Aesthetic}**, **DAS_{Aesthetic}**, **DEMON_{Aesthetic}**, and **DNO_{Aesthetic}**. For prompts: “A comic book illustration by John Kirby depicting a jungle fortress surrounded by dirt walls in a marketplace setting with cinematic rays of sunlight.”, “The smooth, glossy finish of the ceramic vase accentuated the vibrant colors of the flowers, a stunning centerpiece of beauty.”, “A black and white photo of a steam of flowers inside a vase.”, “An airplane on the runway of an airport.”, “A girl is holding a large kite on a grassy field.”

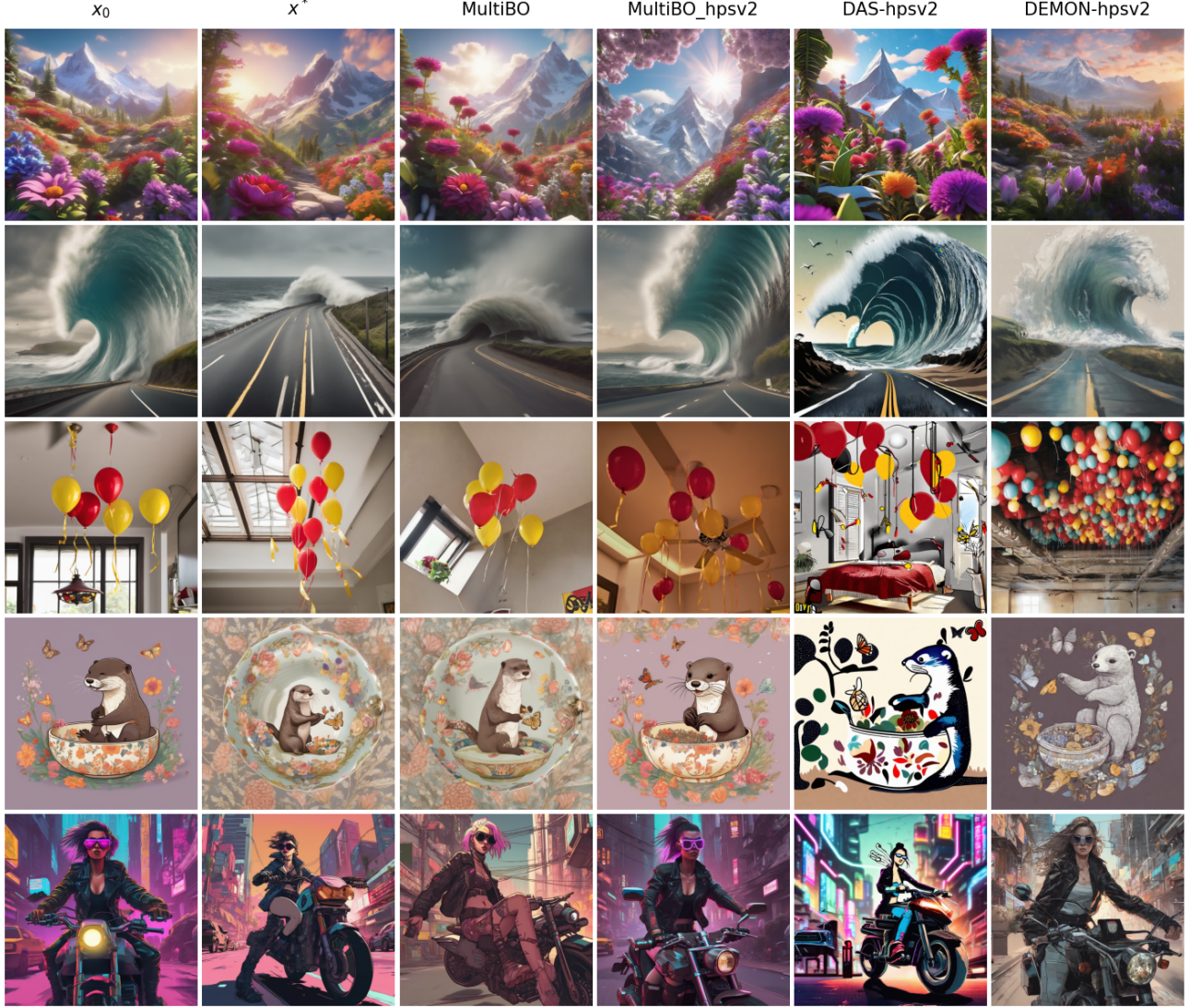


Figure 14. Qualitative results comparing **MultiBO** ($B = 50$), **MultiBO_{HPSv2}**, **DAS_{HPSv2}**, **DEMON_{HPSv2}**, and **DNO_{HPSv2}**. For prompts: “a stunning 3d render of towering, giant blooming plants with vibrant, colorful flowers on a picturesque mountain landscape. sunlight dances on the petals, creating an enchanting scene as the wind gently sways the plants, with snow-capped peaks in the distance.”, “a tidal wave approaching a coastal road”, “red and yellow balloons hanging from a ceiling fan”, “A flower patterned otter is playing with a butterfly shaped bowl”, “A cyberpunk woman on a motorbike drives away down a street while wearing sunglasses.”

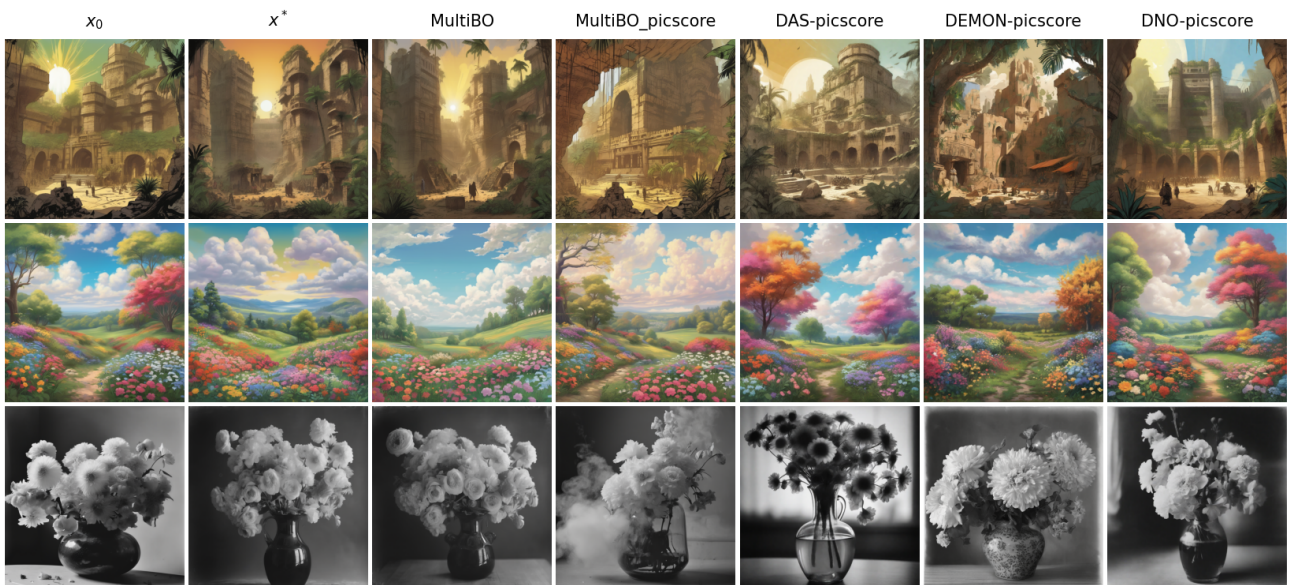


Figure 15. Qualitative results comparing **MultiBO** ($B = 50$), **MultiBO_{PicScore}**, **DAS_{PicScore}**, **DEMON_{PicScore}**, and **DNO_{PicScore}**. For prompts: “A comic book illustration by John Kirby depicting a jungle fortress surrounded by dirt walls in a marketplace setting with cinematic rays of sunlight.”, “A peaceful, nature-filled landscape with vibrant flowers and trees and a serene cloud-filled sky.”, “A black and white photo of a steam of flowers inside a vase.”

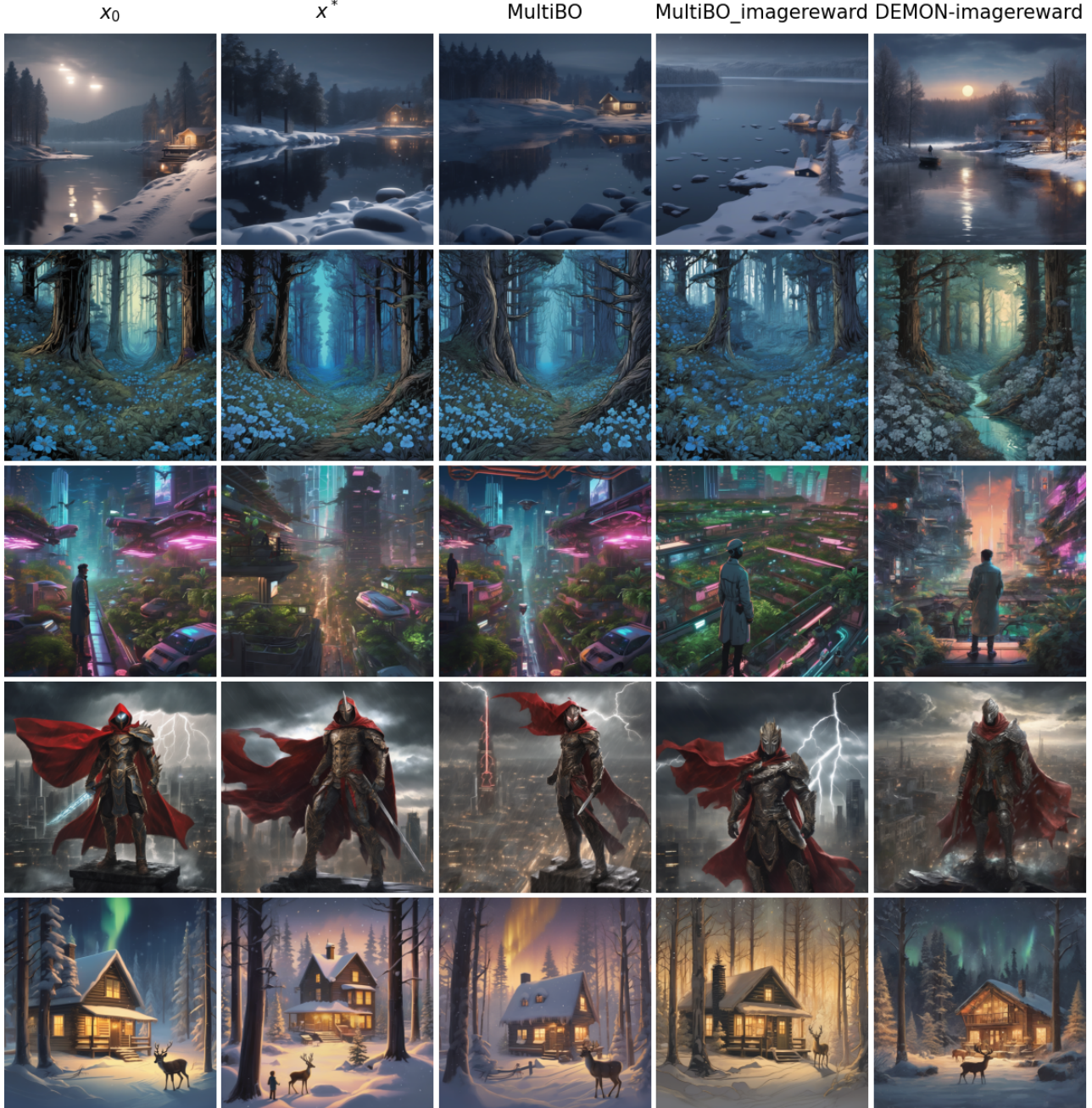


Figure 16. Qualitative results comparing **MultiBO** ($B = 50$), **MultiBO_{ImageReward}**, **DEMON_{ImageReward}**. For prompts: “A vividly realistic depiction of a snowy Swedish lake at night with hyper-detailed, cinematic-level artistry showcased on ArtStation.”, “A forest with blue flowers illustrated in a digital matte style by Dan Mumford and M.W Kaluta.”, “On the rooftop of a skyscraper in a bustling cyberpunk city, a figure in a trench coat and neon-lit visor stands amidst a garden of bio-luminescent plants, overlooking the maze of flying cars and towering holograms. Robotic birds flit among the foliage, digital billboards flash advertisements in the distance.”, “Amidst a stormy, apocalyptic skyline, a masked warrior stands resolute, adorned in intricate armor and a flowing cape. Lightning illuminates the dark clouds behind him, highlighting his steely determination. With a futuristic city in ruins at his back and a red sword in hand, he embodies the fusion of ancient valor and advanced technology, ready to face the chaos ahead.”, “A cozy winter cabin in a snowy forest at night. Warm yellow lights glow from the windows, and smoke gently rises from the chimney. A deer stands near the trees, watching as a child builds a snowman. In the sky, the northern lights shimmer above the treetops.”



Figure 17. Qualitative Examples when **MultiBO** falls short of reaching x^* in $B = 50$ iterations. For prompts: “Psytrance artwork featuring octane design.”, “Beautiful flowering plant with big flowers.”, “an electron cloud model is displayed in vibrant colors with a light spectrum background, showcasing the probability distribution of electrons around the nucleus. the image resembles digital art with pixelated elements, bringing a modern, educational twist to atomic structure visualization.”, “The soft, fluffy clouds drifted lazily across the blue sky, a canvas of endless possibilities and imagination.”, “The smooth silk gown flowed over the delicate skin and the rough floor.”